2017-01-01

Advances in Chemical Vapor Deposition Growth of Molybdenum Disulfide for Photodetectors and Flexible Electronics

Carlos Francisco De Anda Orea
University of Texas at El Paso, cfd.andor@gmail.com

ADVANCES IN CHEMICAL VAPOR DEPOSITION GROWTH OF MOLYBDENUM DISULFIDE FOR PHOTODETECTORS AND FLEXIBLE ELECTRONICS

CARLOS FRANCISCO DE ANDA OREA

Master's Program in Electrical Engineering

APPROVED:

Anupama B. Kaul, Ph.D., Chair

Deidra R. Hodges, Ph.D.

Paras Mandal, Ph.D.

Yirong Lin, Ph.D.

Charles Ambler, Ph.D.
Dean of the Graduate School

DEDICATION

I would like to dedicate this thesis to my academic role models my parents Dr. Joaquina Orea Lara and Dr. Francisco J. de Anda Salazar for always giving me the liberty to choose the pad I want to follow. And special dedication to Dr. Anupama B. Kaul, who not only share valuable knowledge in synthesis of materials, nanotechnology and fabrication processes, but also taught me how to be a hard worker through her example.

I also would like to dedicate this work to, my aunts Alva Orea Lara, Irene Amador Gonzalez and my uncles Gildardo Orea Lara and Juvenal Orea Lara, for always serving as inspiration and support for all projects I have started, Thanks for never let me doubt myself.

ADVANCES IN CHEMICAL VAPOR DEPOSITION GROWTH OF MOLYBDENUM DISULFIDE FOR PHOTODETECTORS AND FLEXIBLE ELECTRONICS

by

CARLOS FRANCISCO DE ANDA OREA

B.S. in Mechatronics Engineering

THESIS

Presented to the Faculty of the Graduate School of

The University of Texas at El Paso

in Partial Fulfillment

of the Requirements

for the Degree of

MASTER OF SCIENCE

Department of Electrical and Computer Engineering

THE UNIVERSITY OF TEXAS AT EL PASO

December 2017

ACKNOWLEDGEMENTS

First of all, I would like to thank my thesis advisor Dr. Anupama B. Kaul, because she was an excellent mentor, who always provided valuable feedback making the research labor much more interesting and enjoyable. In addition to it, her leadership is an example of dedication and love for work. She always transmits the philosophy of hard work and excellence, by encouraging us to move forward, even towards the unknown, because that is how the excellence is reached. Her background in research field makes me feel really proud that she is my thesis advisor. Without her valuable ideas and funding this work would not be possible.

In the same way I would like to thank Dr. Deidra R. Hodges, Dr. Yirong Lin, and Dr. Paras Mandal for accepting to be part of my committee. I am so glad to have such a professional team as my thesis committee and their feedback really improved the quality of this work. Primarily, Dr. Hodges's feedback because she is a specialist in photovoltaic devices, her comments were taken with special attention to improve the quality of the work.

I also would like to thank my friend Gustavo A. Lara Saenz (Ph.D. candidate) for helping me doing the optoelectrical measurements in such a complex cryogenic probe station, and for all his guidance and tutoring he provided during this work. He is an example of professionalism and dedication and also a hard worker. Driven by the ideal of progress, he is always willing to help and contribute to improve any assignment as best as possible. In addition to it, I also want to thank Dr. Kaul's entire research group at UTEP: Thanks to Dr. Misook Min, Jorge Catalan, Avra Bandyopadhyay, Ridwan Hossain, Jay Desai and Srishti Chug for all the valuable feedback during all group meetings.

ABSTRACT

The conversion of light into electrical signals is at the basis of technologies that affect our daily lives. Applications, including video imaging, optical communications, biomedical imaging, security, night-vision, gas sensing and motion detection have reached a high level of maturity due to the development of high-performance materials, large-scale production, and integration technologies. Currently conventional photodetectors made of Silicon (Si) or III-V compounds are about to reach their maximum efficiency, and every time it is harder to get a noticeable improvement in performance of sensors based on these materials, not to mention the complicated fabrication methods to achieve just a few increments in efficiency. This is due to their intrinsic properties. For instance, Si has an indirect band gap, besides Si creates crystal lattice vibrations called "phonons" instead excitons or electron-hole pairs (*aka* "e-h pairs"), when photons are absorbed over the metal surface, these phonons make the switching slow between on and off states. GaAs is also more sensitive to light intensity, but high-performance Ga based photodetectors has reached values in responsivity around ~ 19.1mA/W and external quantum efficiency of 15% for a GaA nanosheet

At the same time, the discovery of graphene in 2004 with its amazing properties, has turned attention to the development of revolutionary graphene based photosensors. In spite of the great improvements that graphene derives in photoconductivity, it is still difficult to achieve high values of efficiency due to the lack of natural bandgap on graphene. However, it has opened the door to a new functional class of 2D materials called Transition Metal Dichalcogenides (TMDs), which in contrast to graphene or silicon, where the electronic properties are based on hybridization of "s" and "p" orbitals, the electronic structure of TMDs depends on the filling of "d" orbitals of the transition metals. The natural bands of energy in 2D TMDCs due to the "d" orbital contribution, leads to sharp peaks in the density of states at particular energy (known as Hove Singularities). When the energy interval between the van Hove singularities of the conduction and valance bands matches the energy of incident photons, the photocurrent generated can be significantly enhanced

up to ~80 according to Yin *et al*. In this work, attention is focused on MoS_2 (Molybdenum disulfide), which is one of the most promising TMDCs analogous to graphene. However, the main difference between these two 2D materials is the electronic properties. While graphene shows semimetal properties due to the lack of bandgap, MoS_2 single layer (SL) has a natural semiconducting behavior having a direct bandgap of around 1.8 eV, which makes MoS_2 SL suitable for transistor and photodetector applications. For being able to understand the capabilities of MoS_2 and be able to notice the huge properties of this material, we fabricated a MoS_2 based photodetector starting from the synthesis of the material. Then, some fabrication methods are applied in order to notice the reduction of processes compared with current heterostructure based photodetectors. The enhancement of this photodetector is supported by taking advantage of the Surface Plasmon Polarization, which are coherent oscillations in the electrons that activate when an electromagnetic wave (EMW) hits a metal structure that corresponds in size to the wavelength of the EMW which greatly enhances the absorption of light. Finally, some optical and electrical characterization are performed to make evident the enhancement before and after nanoparticles. In this work these measurements showed an increment in photocurrent of at least three orders of magnitude going from 2 $x10^{-7}$ Amperes before Au NP deposition, to 2 x 10^{-4} Amperes after Au NP deposition for broadband as light source. In the case of narrow-band measurements for laser at 660 nm an increment in photocurrent of 5 orders of magnitude was seen in going from 3.7 $x10^{-9}$ Amperes all the way to 1.6 $x10^{-4}$ Amperes. This work shows the enhancement in performance seen with Au quantum dots, as also validated by External Quantum Efficiency (EQE) measurements, which show an increment in EQE of 76 times at 550nm wavelength where the efficiency increased from 9.7% before adding Au NP to 735% efficiency after adding Gold NPs. These enhancements in optical absorption efficiency are attributed to the plasmonic effect which can prove to be vitally important for a number of applications platforms such as detectors or solar cells

TABLE OF CONTENTS

LIST OF TABLES

LIST OF FIGURES

CHAPTER 1: INTRODUCTION

1.1 2D materials and Transition Metal Dichalcogenides properties

The discovery of the outstanding properties of graphene in 2004 has been the breakthrough in many research fields that has attracted special interest in two-dimensional (2D) layered materials. The characteristic of these materials is a strong in-plane covalent bonding and a weak out-of-plane van der Waals bonding that allows the isolation of single layer with one atom thickness, just like graphene. However, graphene acts as a semi-metal due to its lack of bandgap, limiting its application in electronic devices. As a result, a whole family of 2D materials has been explored, obtaining special attention the Transition Metal Di-Chalcogenides (TMDCs) due to its semiconductor behavior with outstanding light-matter interactions suitable for optoelectronic applications. TMDC's are compounds made of a transition metal (symbolized as M) atom which is sandwiched between two chalcogens (symbolized as X) atoms, giving the stoichiometric MX2, where M stands for a transition metal (e.g. W, Mo, and Nb), sandwiched by chalcogenide atoms X (e.g. S and Se). TMDCs electronic properties are strongly related to the number of atomic layers, this characteristic allows a tunable bandgap according to the number of layers. The most remarkable is the Direct Bandgap which is reachable only for Single Layer TMDCs, this property can be used to build "interband tunnel FETs" which offer lower power consumption than classical transistors.

In contrast to graphene or silicon where the electronic properties are based on hybridization of "s" and "p" orbitals, the electronic structure of TMDs depends on the filling of "d" orbitals of the transition metals. The natural bands of energy in 2D TMDCs due to the "d" orbital contribution, leads to sharp peaks in the density of states at particular energy (known as Hove Singularities) for MoS_2, WS_2 and WSe_2 these singularities happen close to the conduction and valence band edges. Therefore, a photon with energy close to the bandgap has higher probability to excite an electron-hole pair due to the large availability of empty states given by the diverging Density of States (DOS) at the singularity. Thus, despite of the reduced thickness of 2D TMDCs (yielding the high transparency) they strongly interact with light because atomic TMDC thickness is responsible for

quantum confinement effects in the out of plane direction resulting in strongly bound excitons increasing absorption efficiency. In addition to it, 2D Materials have remarkable elastic modulus and large strain (>10%) before rupture, the strain can be used to tune optical properties and realize novel device architectures (wearable, bendable devices) and novel functionalities, like exciton tunneling. Table 1 shows some of the differences between conventional Photodetectors Si based and new 2D TMDCs based Photodetectors reported

Table 1.1. comparison between conventional Silicon based photodetectors and 2D TMDCs photodetectors.

Property	**3D (conventional) photodetectors**	**2D (TMDCs) Photodetectors**
bandgap	indirect	Direct (and tunable)
Channel	Thick (Opaque)	Thin (transparent)
Thin (transparent)	Low young modulus Si~ 180 GP (Brittle)	High young modulus MoS2~3.7 TP (High strain)
Manufacturing process	several chemical processes (harmful to environment)	Less chemical process (less impact to environment

1.2 MoS_2 properties

One of the most promising TMDCs is the molybdenum disulfide (MoS_2). Which is part of the 2D materials pallet: Graphene(conductor), Boron Nitride (insulator) Molybdenum disulfide

`

(semiconductor). MoS_2 is one of the most extensively studied among the various transition-metal dichalcogenides due to its electrical and mechanical properties. Meanwhile Bulk MoS_2 has been used for several decades in industry as a solid lubricant or an additive for lubricating oils and greases thanks to its weak van der Waals forces in the out of plane bonding[1] [2] MoS_2 single layer is well known for its electric properties attributed to the quantum confinement and surface effect [3].

There are 4 polytypes of MoS_2 that have been currently identified (1H, 2H, T, 3R), its different morphologies are related to the anisotropic structure of MoS_2, which is a consequence of its chemical bonding. These structures that predominantly expose the edges of the layers exhibit high surface energy. Such edge-terminated films are metastable structures of MoS_2, lead to diverse catalytic applications [4], [5] in hydrodesulfurization catalysis[6], hydrogen evolution reaction, lithium storage[7], lithium batteries [3] as well as for some biological applications.

This work is focused on 1H-MoS_2 because this is the most stable type among all polytypes [8], [8], and also because of its unique Mechanic, Optic and Electronic properties, such as: mechanically flexibility with a Young's modulus of 0.33 ± 0.07 TPa [7] such property allows MoS_2 be stained up top 10% (similar to graphene), as well as Direct bandgap (Single Layer) of 1.8eV which makes MoS_2 good for switching nanodevices. 1H-MoS_2 is a crystal conformed by weakly coupled layers of S-Mo-S, where an Mo atom layer is sandwiched by two layers of S atoms (Mo atom is separated approximately 2.41 Å from each S atom). Each Layer of MoS_2 are about 3.15Å thick, hexagonally packed with a distance between layers of 3.49 Å, as it can be seen in Figure 1. These layers could move relatively easy against each other due to the weak van der Waals interactions.

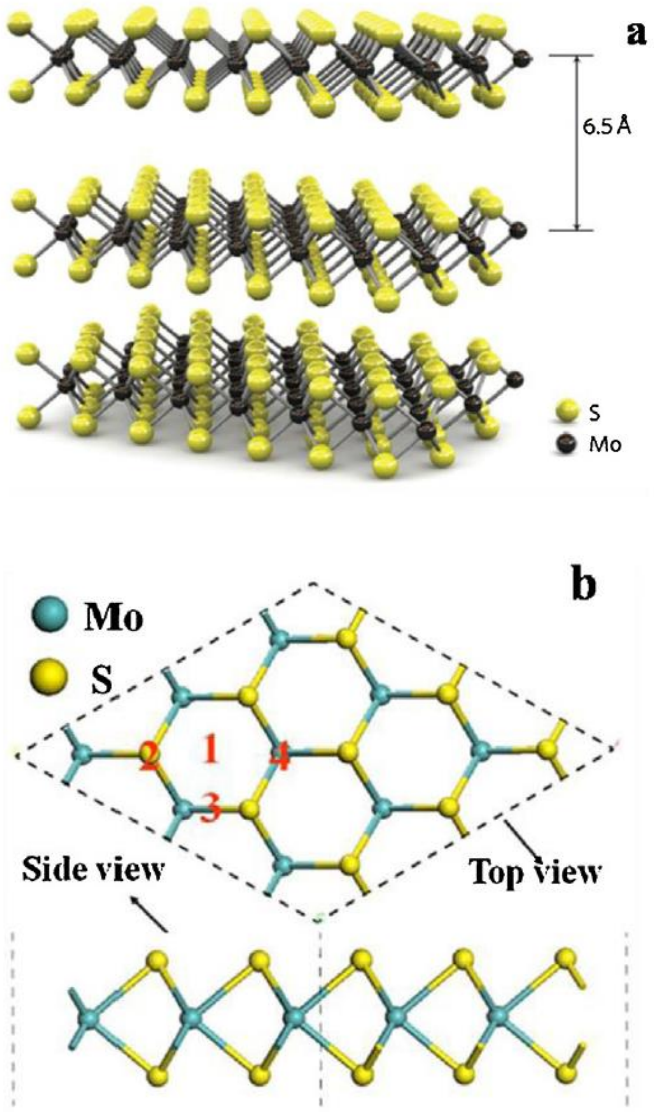

Figure 1. Image from "Molybdenum Disulfide nanomaterials structures, properties, synthesis, and recent progress on hydrogen evolution reaction" by Zuoli He [9]. a) A 3D representation of the structure of 1H-MoS_2 is seen, and b) is a schematic of the hexagonal crystal lattice with honey comb structure packed structure optimized with four absorption sites.

The unique electric properties of MoS_2 are due to the large band edge exciton of the metal centered d-d transition. In MoS_2 the conduction band minima (CBM) trade place in terms of energy, leaving the k-point CBM directly above the valence band minima (VBM) which is increased by approximately 100meV, converting the bandgap for a single layer from indirect to direct. this can be appreciated in figure 2 [8].

`

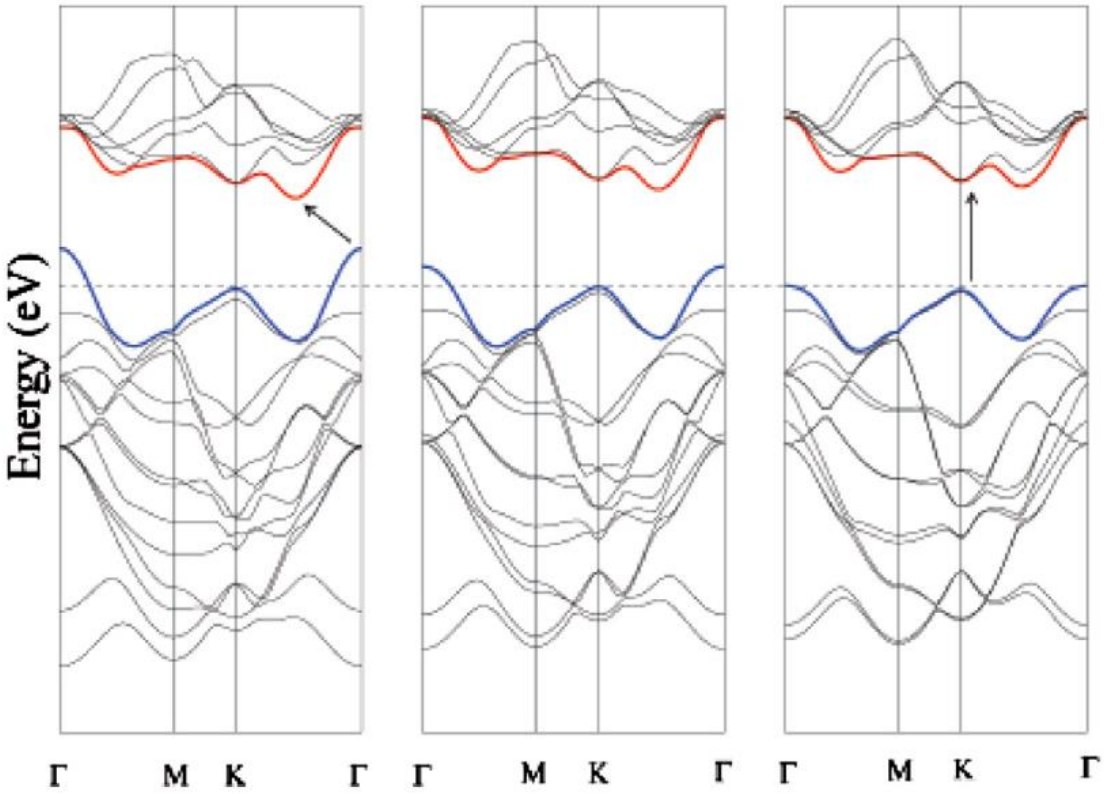

Figure 2. Obtained from Electronic Properties of MoS_2 Nanoparticles by Tianshu Li and Giulia Galli [10]. Variations of the bandgap in multilayer MoS_2 sheets with respect to: a) the number of sheets n, and b) separation distance w (referring to the z axis distance between the upper S layer of sheet B and the lower S layer of sheet A, note that sheets A and B contain tree atomic layers S-Mo-S).

1.3 Characterization methods

1.3.1 Optical Microscopy

Optical identification of single layer and multilayer MoS_2 Nanosheets is possible thanks to the Hai Li group who developed a simple rapid and reliable optical method to identify the single to five layer (1L-5L) nanosheets based on the optical contrast of the MoS_2 Nanosheet like in the image (3). The contrast difference between the 2D nanosheet and substrate can be simply obtained from the brightness profile of their color images or grayscale images of the R, G, or B channel that they later confirm by AFM. Hai Li's group developed a chart Contrast Vs layer number based on image software analysis according to the different values of contrast giving by the AFM (3q).

`

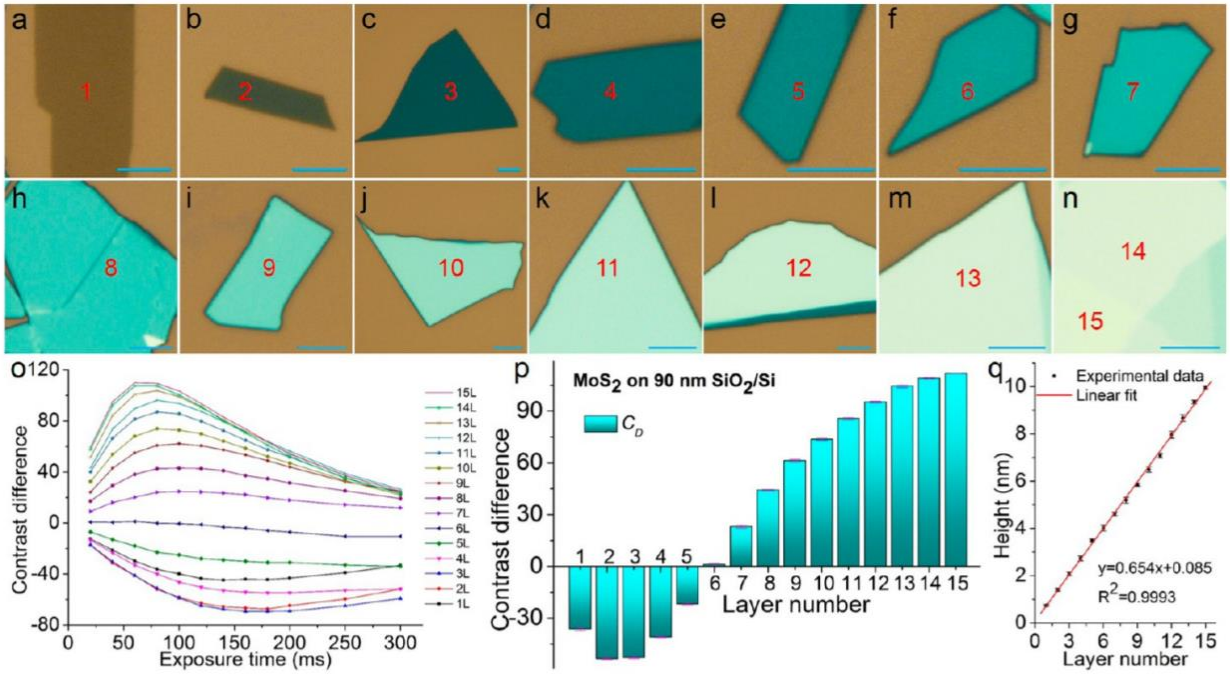

Figure 3. image from Rapid and Reliable Thickness Identification of Two Dimensional Nanosheets Using Optical Microscopy by H. Li. From [8] a) to n) optical images of films of one plus one layer thick and so on starting from one layer all the way to fifteen layers, O) shows a relationship between contrast among SiO_2 90 nm and film contrast using image-J software, p) shows the relationship between contrast and number of layers, and q) is a plot of the thickness from 1L to 15L MoS_2 nanosheets measured by AFM.

1.3.2 Raman Spectroscopy

Raman spectrometry is a characterization method to illustrate the evolution of structural parameters in layered materials in changing from 3D bulk blocks to 2D van der Waals bonded constructions typical Raman peaks, known as E_{2g}^1 and A_{1g}, are indicated to describe the crystal structure. Raman spectroscopy is based on the scattering of light by molecules, each molecule has different ways to vibrate and this vibration changes depending on its shape. Vibrations are associated with particular energy levels. The molecule can only exist long-term in one of these set modes, when light interact with molecule, the molecule can receive energy from an incoming packet of energy known as a photon which promotes up to a higher energy. If this doesn't match

one of the modes of the molecule it immediately goes back down to release a photon. There are three things that can happen when photon hits the molecule:

1. Elastic Scattering; in the majority of cases the molecule relaxes back to its original vibrational state.
2. Stokes Raman; is an inelastic effect that takes the molecule into a upper level energy (higher energy photon).
3. Anti-Stokes Raman; is another inelastic effect that takes down the molecule into a lower energy state (lower energy photon).

These 3 possible effects are shown in a schematic in Figure 4.

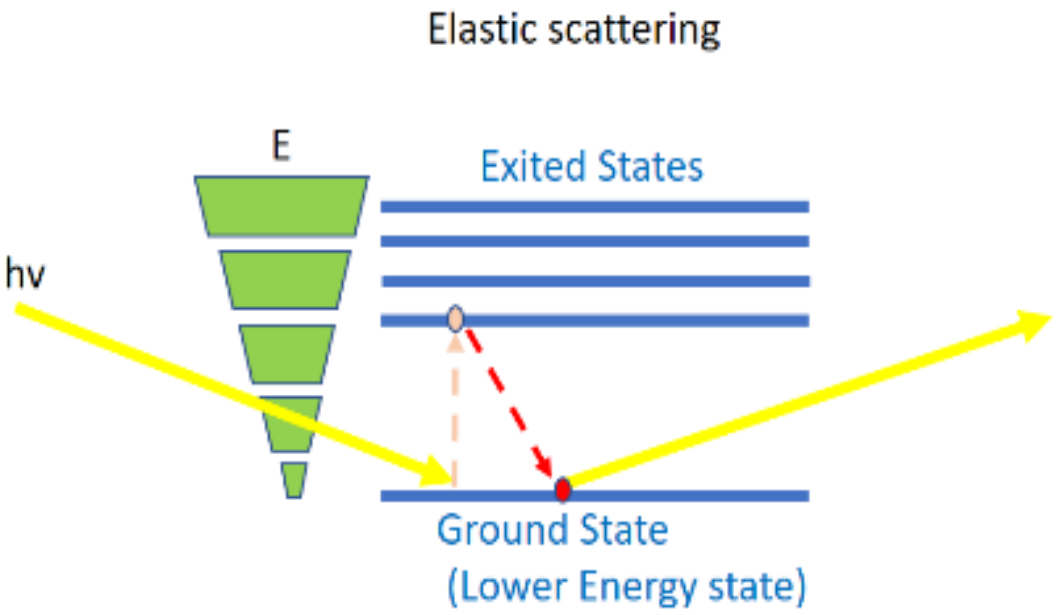

Figure 4. light-molecule interaction showing a) elastic scattering where the photon energy in and out is the same.

`

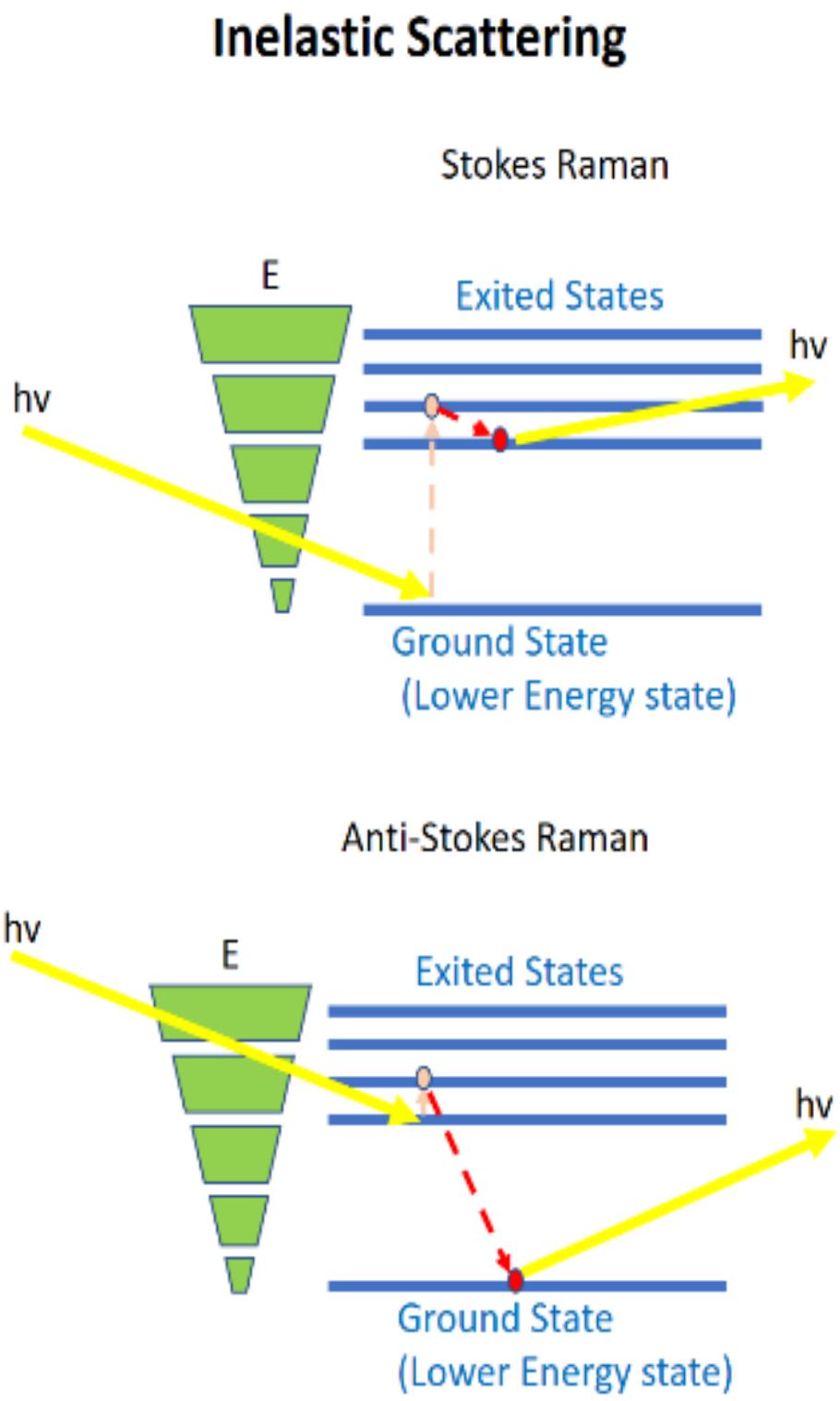

Figure 5. b) and c) are both inelastic scattering, the firs one is known as Stroke Raman and means the energy getting out is bigger than the energy geting in, meanwhile for the later the energy getting in Is lower than the energy getting out.

`

Since inelastic scattering occurs one in every million scattering events (which means that molecule spontaneously relaxes to a vibrational energy state which is higher or lower than the original state) the energy levels of the molecule can be determined by measuring the difference in energy of the outgoing photon compared to the energy of the incoming photon. The energy levels are unique to each molecule so they act as a finger print allowing the molecules in the sample to be determined.

Raman spectroscopy measurement is carried out to probe the layer thickness and the crystal quality of the MoS_2 film. Two typical peaks corresponding to the out-plane vibration of Sulfur atoms named A1g appears at ~403.0 cm^{-1} and in plane vibration of Mo and S atoms (since MoS_2 has 2 S atoms) known as E^1_{2g} appearing at ~384.0 cm^{-1} [11]. These two peaks vary depending on the thickness of the film, meaning there is more or less layers of the material, we can determine the number of layers by the frequency distance Δk which for monolayer must have a value around 19.9 cm^{-1}.

`

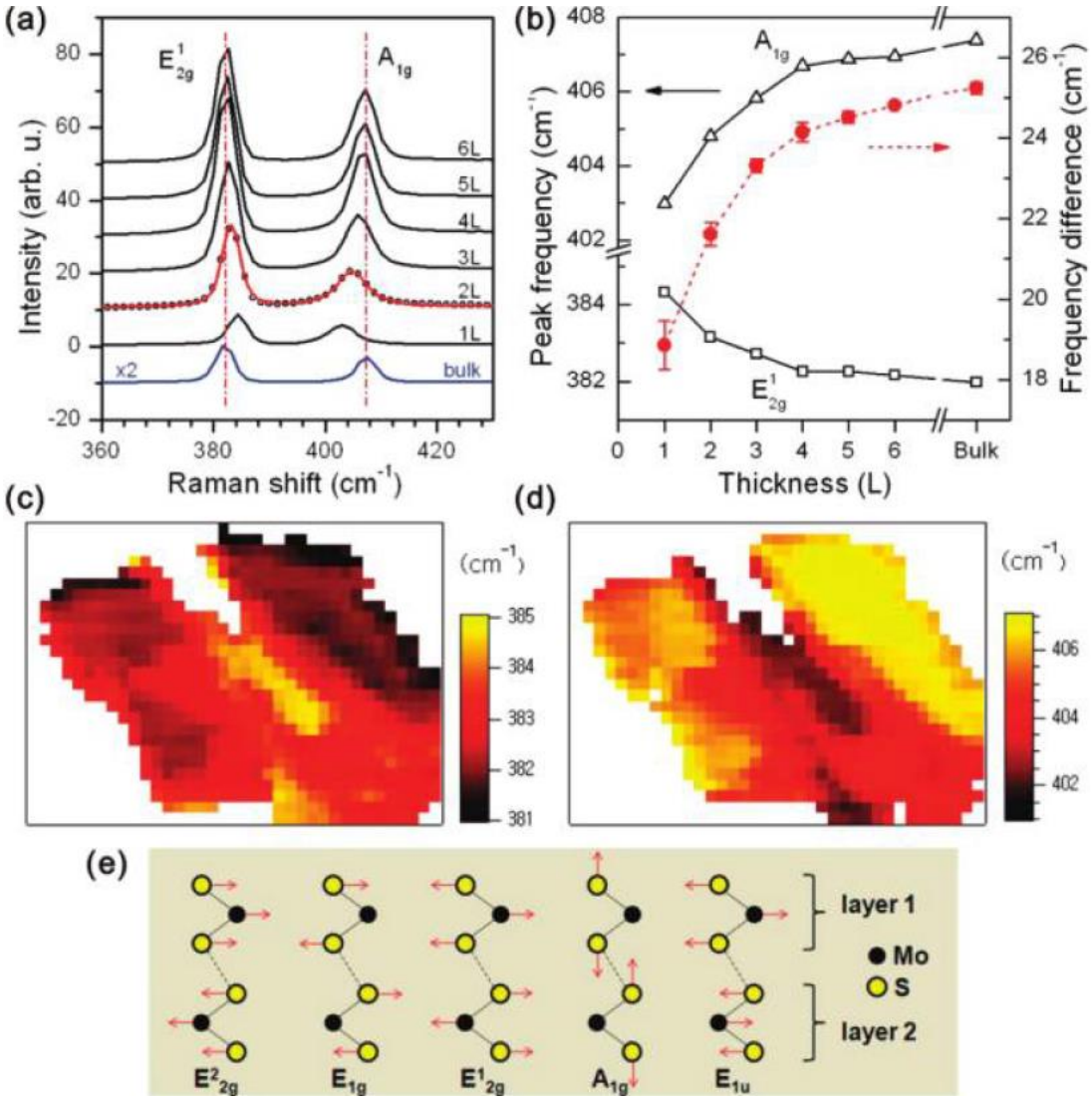

Figure 6. Image from Anomalous Lattice Vibrations of Single and Few-Layer MoS_2 by Changgu Lee[11], showing the relationship between the Frequency difference "ΔK" and the number of layers, it can be seen in a) multiple Raman Spectra from 1L to 6L supporting the graph in b) where it is shown the direct relation between the number of layers and Δk. c) and d) are spatial map of Raman of the Raman frequency of E^1_{2g} and A_{1g} modes respectively for the sample in film e) Atomic displacements of the four Raman-active modes and one IR-active mode (E1u) in the unit cell.

`

1.3.3 Photoluminescence (PL) Spectroscopy

Photoluminescence is the absorption and re-emission of photons by a material, this effect happens because electrons in atom are arranged in discrete energy levels. Energy of the incoming photon causes the electron to jump from the lower energy level to the higher energy level.

Photoluminescence Spectroscopy is a contactless and nondestructive method for probing the electronic structure of materials. It uses a light beam that is focused directly to the sample which will interact by a process called Photo-excitation. The energy will be absorbed for the material and some part of that energy will be dissipated by the sample trough the emission of light. Photo-excitation causes electros within a material to move into permissible excited states. When the electrons return to their equilibrium states, the excess energy is released and may include the emission of light or may not. The energy of the emitted light (AKA photoluminescence) is related to the difference in energy levels between the two electron states involved in the transition between the excited state and the equilibrium state.

Photoluminescence is closely related to the number of layers in MoS_2 [12]. Distinct PL peaks for different number of layers is reported by Andrea Splendiani [13]. Two characteristic absorption peaks at 670nm and 627nm identified as A1 and B1 exciton peaks can be observed in the spectrum for 1L MoS_2, while they disappear in bulk MoS_2. These excitons are associated with the energy split from valence band spin-orbital coupling. Prominent peaks for 1-layer sample indicate the direct excitonic transitions at the Brillouin zone “K point” which matches with the theoretical prediction of indirect (1.2eV) to direct (1.8eV) bandgap transition from Bulk to monolayer band structure.

`

1.4 introduction to semiconducting Photodetectors

A photodetector is an optoelectronic device that absorbs light energy and convert it into electrical energy, which usually manifests as “Photocurrent”. Physics principle ruling photodetectors is the “Photoelectric effect” (Max Planck, 1900, under the concept of energy Is radiated in small discrete units called quanta). Photoelectric effect is defined as the effect of light over a metal surface in a vacuum, that results in electrons being ejected from the metal surface allowing electron flow (known as current). Using the classical Maxwell wave theory of light, the more intense the incident light the greater the energy with which the electrons should be ejected from the metal. That is, the average energy carried by an ejected (photoelectric) electron should increase with the intensity of the incident light. Later on, Einstein in (1905) successfully was able to explain this phenomenon by proposing that that the incident light consisted of individual quanta, called photons and explain that for a given frequency (or color) of the incident radiation, each photon carried the energy E = hf, where h is Planck's constant and f is the frequency of the electromagnetic wave.

Besides photoelectric effect, photocurrent can also be created by another two mechanisms called photoemissive and photovoltaic, all these 3 mechanisms are the result of light creating an electron-hole pair on the surface of a metal. Regular configuration of photodetectors is the photodiode (a diode is a junction of oppositely doped regions called n or p regions in a sample of semiconductor, this creates a region depleted of charge carriers resulting in high impedance). since photodiodes are diodes using light as external input, these devices operate under reverse bias conditions, where the current through the junction is zero when no light is present, this attribute allows the diode to be used as a switch or relay when sufficient light is present. Examples of devices related to light by the same effect are: solar cells (absorbs light and turn it into energy), LEDs (which is basically the inverse of a photodiode, LEDs convert current or voltage into light. the different types of Photodiodes are mentioned bellow with a short description.

1.4.1 Photodiodes (Schottky diodes or Metal Semiconductor Metal diodes) when photons are absorbed in the metal surface they create electron-hole pairs (aka exciton pairs) in the depletion

`

region, once charge carriers are produced in the semiconductor material the carriers reach the junction by diffusion.

1.4.2 PIN Photodiode; a regular photo diode configuration that includes an intrinsic layer between the P and N type materials. PIN is only reversed bias configurated due to the high resistivity of the intrinsic layer. PIN has larger depletion region which allow more e-h pairs to be created at lower capacitance. PIN diodes have better frequency response due to electron mobility greater than hole mobility. PIN also has larger breakdown voltage in comparison with PN diodes, this allow them to be used with a biases voltage of approx. 100, which make the time response faster.

1.4.3 Avalanche Photodiode; It is oppered close to the breakdown voltage which cause photoexcited carriers to accelerate in the depletion region and produce aditional carriers by an effect called avalanching. This type of diodes are good for fiber optic systems that require aditional low light levels with Q. Efficiency latger than 100%.

1.4.4 Phototransistor; since it is configured as PNP or NPN it can be said that Phototransistors have a photodiode with an internal gain. Phototransistors are represented by a bipolar transistor that is enclosed in a transparent case so that the photons can reach the base-collector junction. The electros generated by photons in the base-collector junction are injected into the base and the current is then amplified. Phototransistors can't detect light any better than photodiodes since they are in the same range. The drawback of a phototransistor is the slower response time in comparison to a photodiode, it is only different configuration as we can see in the Figure 7.

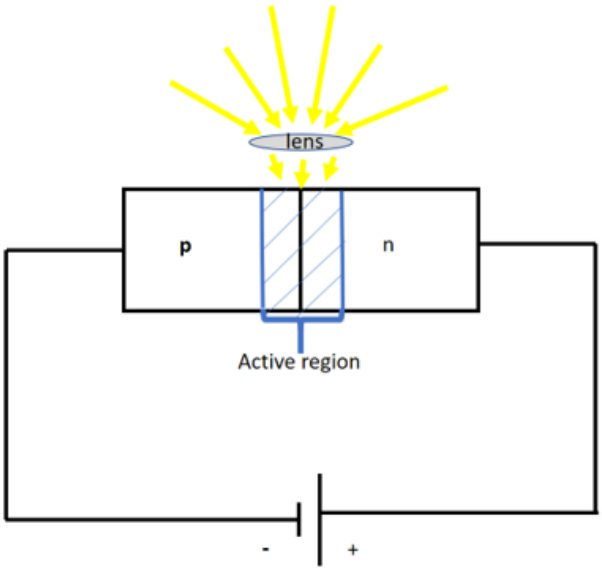

a) Photodiode configuration

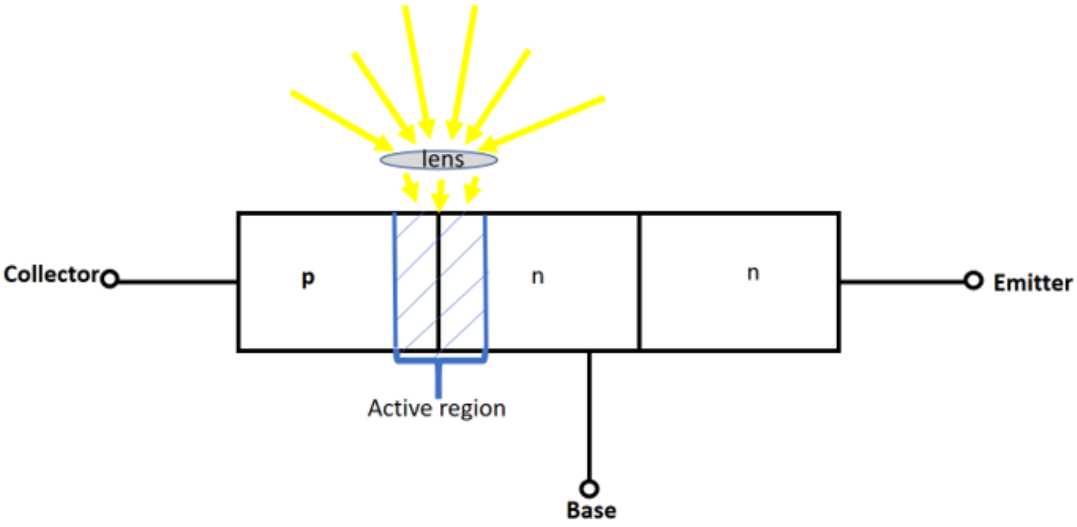

b) Phototransistor configuration

Figure 7. Photodetector configuration a) diode and b) transistor the schematic illustrates that both configurations are almost similar, on the other hand Photodiodes have shown to be more efficient because are faster than Phototransistors.

`

Examples of devices related to light by the same effect are: solar cells (absorbs light and turn it into energy), LEDs (which is basically the inverse of a photodiode, LEDs convert current or voltage into light.

1.5 Plasmonic effect

power conversion efficiency (PCE) is controlled by the absorption of light and the collection of charges at the electrodes. The collection of charges at the metallic electrodes is possible thanks to a phenomenon known as trapping. The light trapping can be achieved with structures that are similar or smaller in size to the wavelength of the light of interest. Metallic nanoparticles have already been studied to enhance the photocurrent and proved an improvement of 33% of for thin film silicon solar cells [14] due to the collective oscillations of electrons in metallic nanoparticles that are generated by the light at a specific frequency leading to a strong absorption or scattering of the light as a function of particle size[15].

When metallic particles are very similar or smaller in size than the wavelength of the light of interest, a strong interaction occurs between the free conduction electrons in the metal and the electromagnetic radiation. Plasmons are the coherent oscillation of these free conduction electrons with the generation of a dipole into the particles due to the interaction with the light. The resonance condition occurs when the frequency of the light matches the frequency of the electrons oscillating and is defined as localized surface plasmon resonance (LSPR) in the case of nanometer sized structures.

The plasmon energy in a free electron model is defined as [Marier, 2007].

$$E_p = \hbar \left(\frac{ne^2}{m\varepsilon_0}\right)^{1/2} = \hbar\omega_p \quad (1)$$

where: n is the density of free electron, e is charge of electron, m is the electron mass, ε_0 corresponds to permittivity of the free space, $\hbar$ is Plank's Constant and ω_p refers to bulk plasmon frequency

According to Harry A. Atwater, Nanoparticles can enhance the absorption of the light by three mechanisms [16]. First metallic nanoparticles can be used as subwavelength scattering elements to couple and trap freely propagating plane waves from the light into an absorbing semiconductor thin film, this is achieved by folding the light into a thin absorber layer; Second, metallic nanoparticles can be used as subwavelength antennas in which the plasmonic near-field is coupled to the semiconductor, increasing its effective absorption cross-section; Third, a corrugated metallic film on the back surface of a thin photovoltaic absorber layer can coupling light into a surface plasmonic polarization mode supported at the metal/semiconductor interface as well as a guided mode in the semiconductor slab, where the light is converted to photocarriers in the semiconductor, shows the possible arrangements of metal nanoparticles on a thin film photodetector for taking advantage of the 3 different mechanisms happening in metal nanoparticles that make able the improvement of photodetectors performance by plasmonic effect.

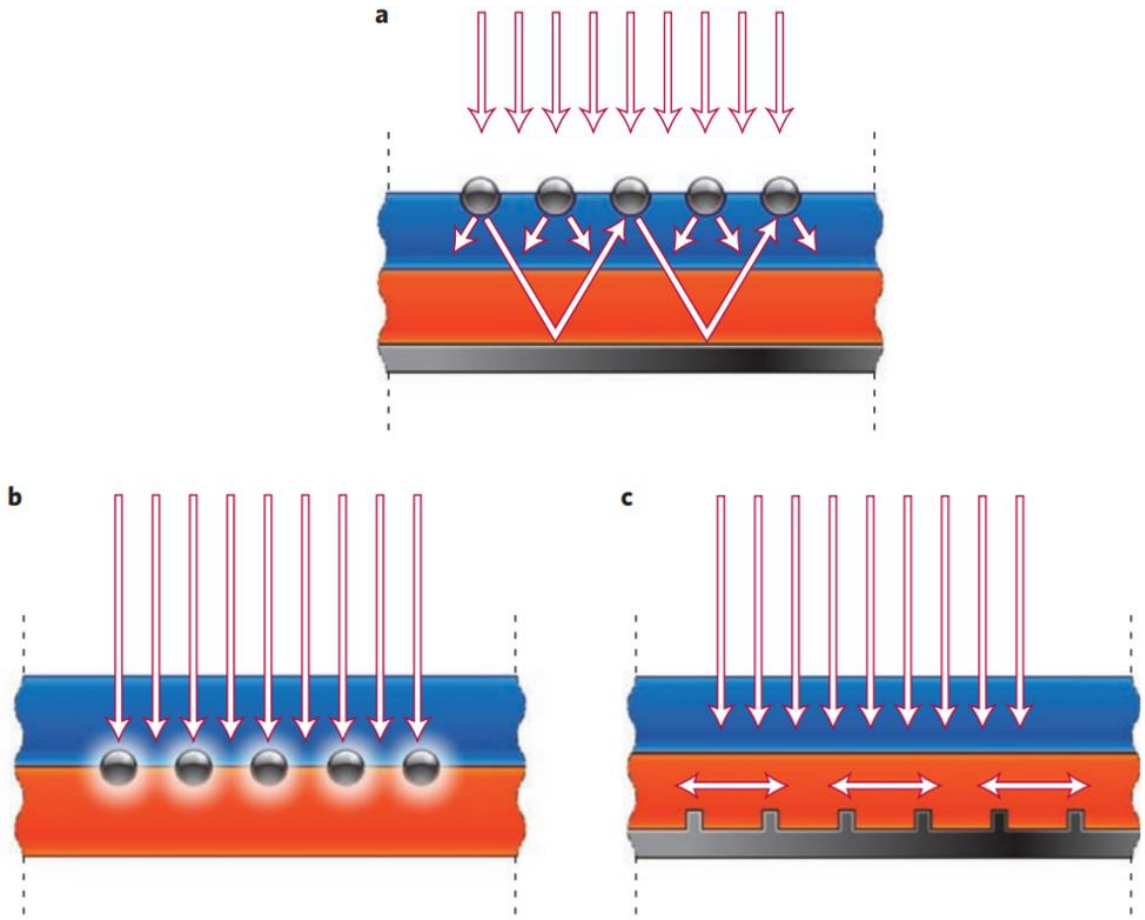

Figure 8. Image from [16] plasmonic light-trapping geometries for thin-film solar cells a) light trapping by scattering from metal nanoparticles at the surface of the solar cell light, b)light trapping by excitation of localized surface plasmons in metal nanoparticles embedded in the semiconductor structure. c) Light trapping by the excitation of surface plasmon polarizations at the metal/semiconductor interface.

1.5.1 MoS_2 Photodetector performance

In 2011, Radisavljevic's group proposed a single layer MoS_2 transistor adopting a hafnium oxide as the gate dielectric material in which the mobility of MoS_2 could be up to $200cm^2/(Vs)$ at room temperature with a current on/off ratio to be $1x10^8$ [17]. FETs made of CVD monolayer usually have n-type behavior and current on/off ratio could reach up to 〖10〗^4[18]. LPCVD (Low Pressure CVD) Method under a pressure around 2Torr (2013 by Yifei Yu) has proved to get uniform MoS_2 films of centimeters by changing MoO3 to Molybdenum chloride (MoCl5) as precursors [18] FETs devices based on this type of MoS_2 synthesis usually can reach up to 0.03cm^2/Vs of mobility. 4 years later in 2015 Oriol Lopez group reported ultrasensitive photodetector n-type channel with field effect mobility of $4cm^2/(Vs)$, reaching a photoresponsivity of 880 A/W [17]. Pip heterostructures strained silicon-germanium based diodes InGaAS. Generally, MoS_2 transistors show the n-type behavior, and under incident light control the photoresponsivity could reach 7.7mA/W at gate voltage of about 50V much higher than that in graphene based devices (which are about 1mA/W at the gate voltage of 60 V) [19].

1.6 Motivation for This Work

Currently the market is full of Silicon and III-V element based compounds (i.e. InP, InAs, GaAs) optoelectronic devices, have proved low efficiency compared to TMDCs photodetectors [17] Conventional photodetectors are made of 3D heterostructures Si or III-V semiconductor based which has no direct bandgap, which means they need several fabrication processes to build in the photodevice itself, these fabrication process usually are very expensive since they need High tech equipment, in addition to it the 3D semiconductor materials used are brittle make the photodetector useless for bendable devices. This kind of photodetectors relay on thick channel to achieve sizable responsivities, making the photodetector fully opaque [17]. The power conversion efficiency (PCE), the device time, and the large-scale production are the three main problems that needs to

be solved in the photodetector technology currently. The most important advantage of TMDC based photodetectors over conventional photodetectors is that meanwhile Silicone has an indirect bandgap (1.1ev) that limits the absorption to the visible and near infrared electromagnetic spectrum, atomic thickness of TMDCs allows quantum confinement effects resulting in stronger bound excitons increasing absorption efficiency.

This work it is intended to Improve photodetector functionality at 3 different approaches: efficiency, economic and environmental friendly processes. First and most important is to improve the efficiency of photodetectors, compared to the ones currently in the market, by taking advantage of the plasmonic effect. The second purpose of this work is to decrease the fabrication cost by taking advantage of the direct bandgap materials known as TMDC, which thanks to their properties we can skip several fabrication steps, not only reducing the economic factor of producing photodetectors but also reducing pollution since all the fabrication process nowadays uses very strong inorganic chemicals dangerous for the environment. And Third, Open the door to flexible MoS_2 optoelectronic for bendable or wearable devices by improving the transfer process.

This text will follow a very straight line indented to be easy to understand for everyone so everybody will be able to comprehend the experimental part. The next chapter talks about MoS_2 Synthesis and classifications in this chapter there are introduced some MoS_2 synthesis methods an characterization techniques with the purpose of shown at the end some results obtained in this work. In chapter 3 some fabrication methods are described and results of this work are presented like MoS_2 mechanical exfoliated bottom contacted with Mo by viscoelastic stamping and MoS_2 CVD synthetized top contacted with Au by e-beam evaporator, the in chapter 4 some Electric and optoelectronic characterization (I-V, Photocurrent, resistivity, Quantum Efficiency (external e internal), detectivity) are presented with the aim to compare the final performance of the photodetector made of mechanical exfoliated MoS_2, among before and after Nanoparticles ,

Finally the last chapter (chapter 5) will be conclusions where a short discussion will be held in order to determine the advantages of using this method. For improve photodetectors efficiency.

This work can have an economic impact on industry since it is a process that Improve the Manufacturing Process by looking at Photodetectors made of TMDC 2D Materials by CVD Synthesis. Another contribution of this work is to open the door to flexible optoelectronic devices for bendable or wearable devices. And the most important, Improve Photodetectors by taking advantage of 2D Materials semiconducting properties and Plasmonic Effect.

CHAPTER 2: MOLYBDENUM DISULFIDE SYNTHESIS

2.1 Molybdenum disulfide (MoS_2) synthesis and classification

The success of Graphene synthesis [20] has led to the adoption of these methods to many other 2D materials. Since TMDCs are considered analogous to Graphene or Graphene like materials, most of the methods used to get Graphene are also applied for obtaining TMDCs atomic films with very little variations such as: precursors, pressure or temperature. These parameters must fit the characteristics of each element that compound the material itself. Basically the methods for achieve molybdenum disulfide (MoS_2) Single Layer or Multilayer films can be classified in two main types, the top-down Approach, which starts from the bulk material down to atomic layer films, and the Bottom-up Approach where the main idea is to form the film by nucleations created as a result of chemical processes between precursors, meaning starting from the smallest resources possible like atom reaction, usually in gaseous state, and letting the film grow atom by atom like construction blocks.

2.1.1 Top-down approaches

The flagship of the Top-Down Approaches is the Mechanical Exfoliation Method, in which Graphene successful exfoliation opened the door for the fabrication of other Graphene-like 2D materials like TMDCs, based on a simple “Scotch tape method” This method is popularly used for intrinsic sheet production of MoS_2 layers because it is the easiest and cheapest way to get Monolayer films from the bulk material. Furthermore, exfoliation is not suitable for large scale production due to its low yield as well as the disadvantage of not being able to control sheet size and number of layers. Other Top-Down methods are: Anodic bonding, which allows nanosheets in ranges of size around 10um to several hundreds of microns[21]; Chemical approaches like ion intercalation and solvent-based exfoliation[21]. Electrochemical lithiation discharge from bulk to Nano, as presented by Hua Zhang’s team in 2011 [22].

The Coleman Method, which is a solvent based method using ultrasonication where it is possible to obtain high yield (92%) MoS_2 Metallic behavior called 1T-MoS_2 [23], later, O'Neill's group further optimized Coleman method by adding a solvent based exfoliation method which first reported to obtain a semiconducting 2H-MoS_2 large scale [24]; And finally, Liquid phase exfoliation is a technique that also starts from the bulk material, the average of shapes and sizes is much larger but the quality is reduced. There are 2 ways to exfoliate MoS_2 in liquid solutions; the first one is the Mechanical liquid exfoliation, which consists of DI water and sonication (shearing, stirring, grinding and bubbling). The second way is via chemical solutions or electrochemistry; Lithium is typically used to intercalate between MoS_2 layers and interlayer spacing easing the exfoliation by mechanical treatment like the one used by Fan et al that used a sonication assisted lithium intercalation by 1.5 hours getting very good results [25]. However, this method usually decreases the semiconductor properties due to structural changes during Lithium intercalation.

2.1.2 Bottom-up approaches

Physical Vapor Deposition has been reported a method on growing MoS_2-ti composite by vacuum sputtering using Ti and MoS_2 as targets. However the result is an amorphous MoS_2 structure [26], usually PVD outcome are grain sizes of the 2D material not as high as expected [27]. Molecular beam epitaxy (MBE) is another bottom-up approach, it is indented to be controlled at any time, the equipment is pretty expensive and the outcome is not that higher than the one of CVD. Solution Chemical Process is one of the most efficient production of MoS_2. This chemical method is also the basis of Hydrothermal synthesis [28] and solvothermal synthesis [29] (the difference between these processes is that the precursors solution is not an aqueous solution for the solvothermal synthesis) these processes typically uses molybdate to react with sulfide on a stainless steel autoclave, where a series of complex chemical reactions take place under relatively high temperature, the outcome varies a lot from powder or thin films depending on the preparation details.

`

Plasma Enhanced CVD is a variation of CVD process but a lower range of temperature. Therefore, by using plasma temperature it can be lowered to 150-300 C, and this makes possible the deposition of MoS_2 directly in the substrate, even on plastic substrates[30]; Moreover CVD is the basis of Metalorganic CVD but utilizing organometallic precursors, and it is used in semiconductor industry to produce Single Layer crystal epitaxial films.

Atomic Layer Deposition is a new promising method, since is a CVD based process, controlled by having three chambers, in which each precursor is stored and heated inside an specific chamber. Secondly, when they reach their own fusion point they are released into a third chamber where the substrate is localized. The controlling goes beyond having a system that introduces gases as a sequential and non-overlapping pulses, separated by pursues in between. In each pulse, molecules react with the surface in a self-limiting way. Therefore, it is possible to grow layered materials with high-thickness precision (layer by layer). This method is presented in the Valdivia's reported experiment [29]. The disadvantages of this method are that is very expensive and since it is a new method further research must be done in order to guarantees a successful outcome.

Finally, Chemical Vapor Deposition CVD is considered the most competitive among all the synthesis methods developed currently. The outcome is possible to keep all the properties of the Single Layer MoS_2. CVD makes possible the synthesis of 2D materials on a wafer-scale which shows potential toward practical applications like large-scale integrated electronics. It is considered as a predictable preparation of 2D TMDCs with large area and the basic idea utilizes two precursors typically Molybdenum based compound powder (MoO3, Mo,) and usually pure Sulfur. Both precursors are heated into a quartz tube inside a furnace to reach their specific fusion point at the same time for the reaction to occur. interestingly it is common to see processes where Sulfur is the only one to reach the fusion point since it is lower than Molybdenum fusion point, that is why this process must be called Sulfurization of Mo Based compound instead of CVD. Sulfurization is also a very common method used in research, Sulfurization of Mo and Mo based oxides consist of Mo thin film redeposited in a wafer. Accordingly, to Lain-Jong (2012) this will

be later introduced to a CVD furnace where sulfur will be evaporated at 750C Thermal decomposition of (NH4)2 MoS4.

2.2 Experiment and Results

2.2.1 Mechanical Exfoliation

Mechanical Exfoliation is possible due to the weak van der Walls forces on the out-of-plane regimen. MoS_2 flakes can be produced on a substrate using sticky tape by peeling off the bulk material. As we mentioned before, Mechanical exfoliation is one of the most popular methods in research because it is the easiest and cheapest ways to obtain MoS_2 films, in spite of the fact that it is harder to get a large area of single layer MoS_2 flakes many researches are still using this method nowadays because it is convenient for beginners and basic research. As a matter of fact, those chemical processes have proved to be suitable for large-scale production. However, there is a good reason for keep using Mechanical Exfoliation, which is related to the quality of the material. Bulk MoS_2 is obtained usually for the mines, where it was formed by natural process over a long period of time. Thus, leading into a high purity material. Since Mechanical exfoliation is a process that starts from the bulk material, it is implied as the purest way to obtain MoS_2 because the material is not exposed to artificial chemical or physical process which usually leaves a lot of residuals that could affect the quality of the outcome during the process.

In work Mechanical Exfoliation method was performed to obtain a Few Layer MoS_2 with two objectives, the first one is to use it as a point of comparison against the CVD MoS_2 synthetized in this article. This way we can compare the Raman and PL spectra intensities and according to Changgu Lee [31] the purest material (the Mechanical Exfoliated one) will present the highest intensity. Furthermore, assure that we are getting a high quality MoS_2 film by optical inspection of the spectra intensity. In addition, it is possible to confirm whether it is a good quality material or not by calculating the FWHM (Full Width at Half Maximum) to the Raman Spectra to determine how pure the material is [31]. According to Changgu Lee [31] the highest quality material (the one that was naturally formed and extracted from the mines) usually reaches a value of FWHM up to

$3.7cm^{-1}$. Meanwhile CVD MoS_2 Synthetized starts with FWHM values above $4.3cm^{-1}$ meaning that the shorter the FWHM for MoS_2 films CVD synthetized, the closer to the purest material, which is reflected as high-quality material.

The second objective of using Mechanical Exfoliation method is to obtain a high quality MoS_2 film monolayer or few layer for later in order to create a photodetector. Since the main purpose of this work is to improve the performance of photodetectors by taking advantage of the plasmonic effect, this MoS_2 Film was prepared following the method of Hai Li et al [32]. The process started with the Bulk MoS_2 crystal from Alfa Aesar then a piece of blue tape is contacted by the glue side to the bulk material, after that and taking advantage of the weak van der Waals forces, the blue tape is peeled off from the bulk material, then some films stay in the glue side of the blue tape. The next step is to press this tape against the new substrate in this case a p-type 270nm SiO_2 from University Wafers, some films will remain in the new substrate due to the van der walls force to the substrate, then the blue tape is gently pressed by a cotton swab and finally the blue tape is slowly removed from the new substrate. A schematic of the process is shown in Figure 9. The disadvantage is that the van der Waals adhesion of many TMDCs to SiO_2 . is much weaker than that of graphene, which happens to make the produced flakes very small (usually less than 10um) [33]. Therefore, this process needs to be repeated several times in order to get Single Layer flakes. In Figure 10, a, b and c shows some results obtained from the experiments carried out in this work. Thanks to this data it is possible to compare the performance between a high-quality photodetector made of Mechanical exfoliated MoS2 against a photodetector made of a synthetic process.

`

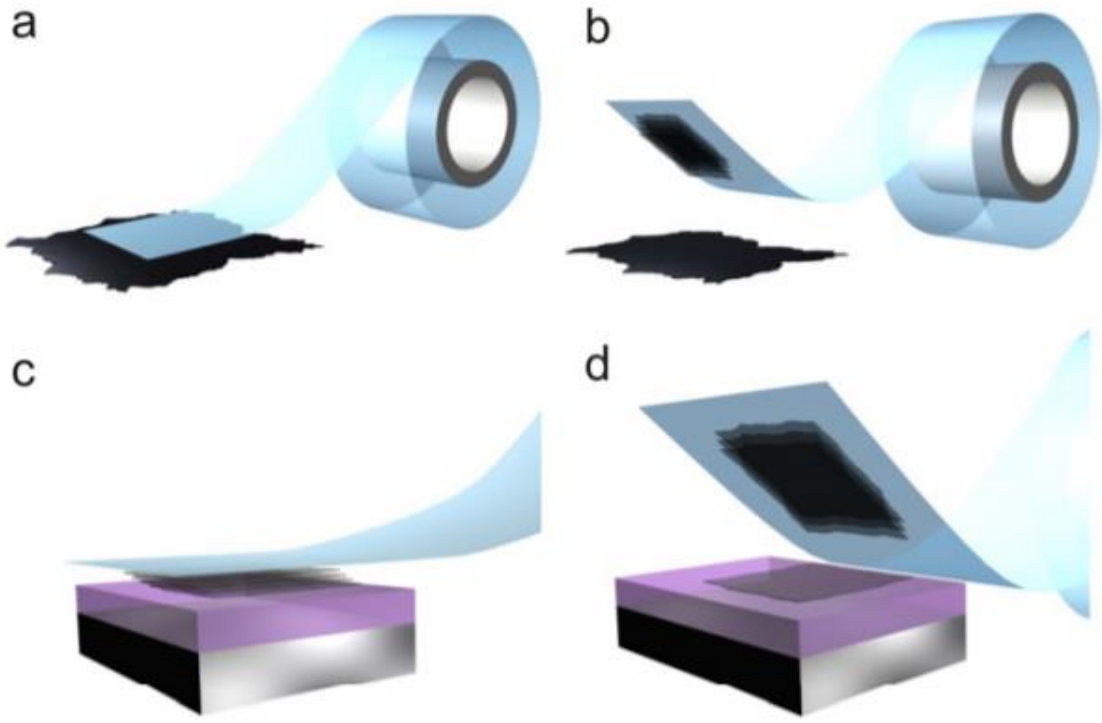

Figure 9. a), b) ,c,) ,d) are the steps for Mechanical exfoliated MoS2, Image obtained from Two-dimensional crystals-based heterostructures: materials with tailored properties by K S Novoselov [34].

`

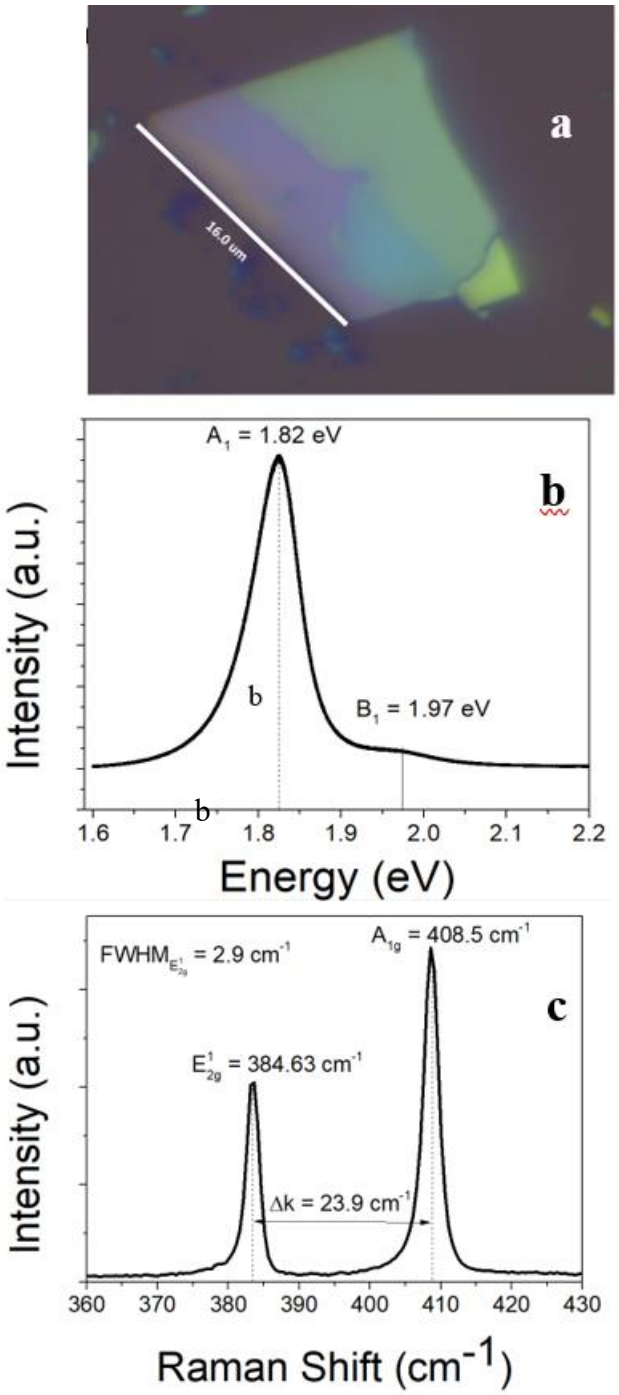

Figure 10. shows some results obtained in this work, a) Optical Image of a MoS_2 exfoliated film presenting 4 types of contrast, the darker one is the one used for characterization b) and c) are Raman and Photoluminescence spectra of the darker area of flake "a".

`

2.2.2 Chemical Vapor Deposition (CVD)

Chemical Vapor Deposition (CVD) one of the most important approaches with capabilities on scalability and high-quality materials. The process for CVD MoS_2 involves two precursors: Sulfur (S) and Molybdenum trioxide (MoO3). These precursors are heated until they reach their fusion points. This method is helped by using a noble gas as a molecule transport. The reaction occurs in vapor phase and then condensed on the substrate surface. Since the synthesis process requires high temperatures, up to 850 ^{o}C. The substrate availability is limited, therefore, SiO_2 is one of the most common substrates for MoS_2 CVD synthesis. Besides the optical contrast that allows the identification of monolayers only with a regular optical microscope. The parameters used in this work are presented in table 2.1

Table 2. most important parameters used in this work for obtaining MoS2 by Chemical Vapor - Deposition process.

Parameter	**Value**
Precursor rate MoO_3:S	1:3
Substrate	270nm SiO2 wafer
Carrier Gas	N2
Flow Rate	~200 SCCM
Atmospheric Pressure	763 Torr
Maximum Temperature	850(MoO3), 600(S)
Distance between precursors	25-27 cm
Time	2-3 hours

`

For this work we use the method of Yi-Hsien Lee [20], which is a APCVD (Atmospheric Pressure Chemical Vapor Deposition). For the purpose of this work the entire process is carried out into the quartz tube of a furnace "OTF-1200X-80SL Sliding Tube Furnace (80mm OD) from MTI corporation" at 760 Torr. Two precursors were used to achieve the reaction, the first one is Molybdenum Trioxide (MoO3) powder by sigma Aldrich and the second one is Sulfur (S) powder 99% by Sigma Aldrich in a ratio about to 1:3. They are placed in two different boats separated around 24 to 25 cm between each other. Another important parameter that was evident thanks to Jianping Shi's group observations, is the distance between precursors which is very important and can highly affect the outcome [35].

In this work it was possible to obtain MoS_2 Single layer films, we can confirm it in Figure 11, where it shows an optical image of the triangular film and next to it the Raman and PL spectra from the flake in "a".

`

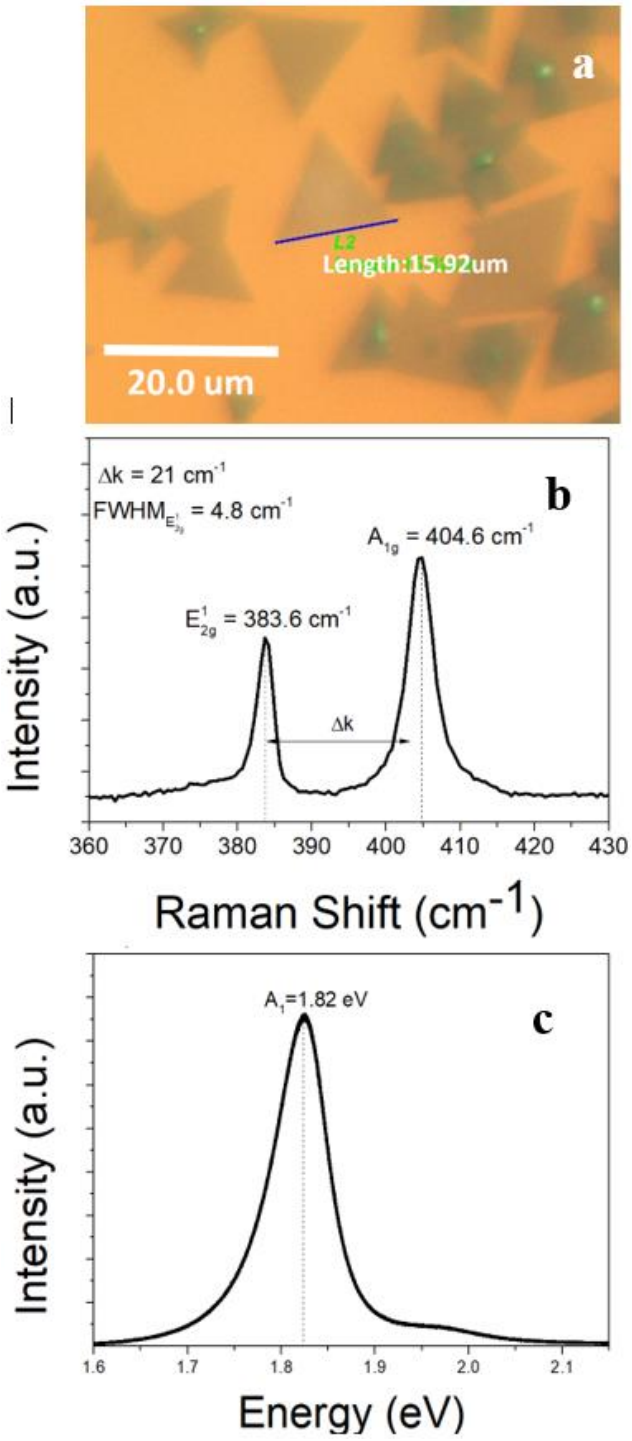

Figure 11. Image a. shows an optical image of a monolayer flake of 15.92um by side, b. and c are the Raman and Photoluminescence of the film in image "a" with a delta k around 21 cm^-1 for Raman and a strong A1 peak for PL confirming that the film is Single Layer.

`

2.2.3 CVD on Sapphire substrate

Aluminum Oxide (Al_2O_3) also known as Sapphire is a chemical compound which is a variation of the mineral corundum considered precious gemstones, it occurs naturally in a crystalline polymorphic phase α-Al_2O_2 but it can be synthetized as well.

For Electronics Sapphire has very useful properties due to its insulator behavior, and other properties such as: thermal conductivity ($30Wm^{-1}K^{-1}$), water insolubility and a crystalline structure which make it suitable for electronic device fabrication [36].

Sapphire is another suitable substrate for CVD due to its surface which provides a good environment for MoS_2 nucleations to growth because it has been probed that nucleation are more like to happen in rough surfaces like defects in the material[37]. In addition to it, Sapphire is the best alternative to growth MoS2 on insulator because it is Catalyst-free substrate which means it doesn't affect the reaction of the two precursors used for CVD Synthesis. This property contributes to make devices right after synthesis avoiding transfer process.

According to Brent D. Keller the crystallinity of Sapphire allows Van der Waals epitaxial growth of graphene like materials. It was observed that the substrate and film grown with van der Waals epitaxy are rotationally commensurate, in spite of the fact that their lattice constants are usually incommensurate with each other [38].

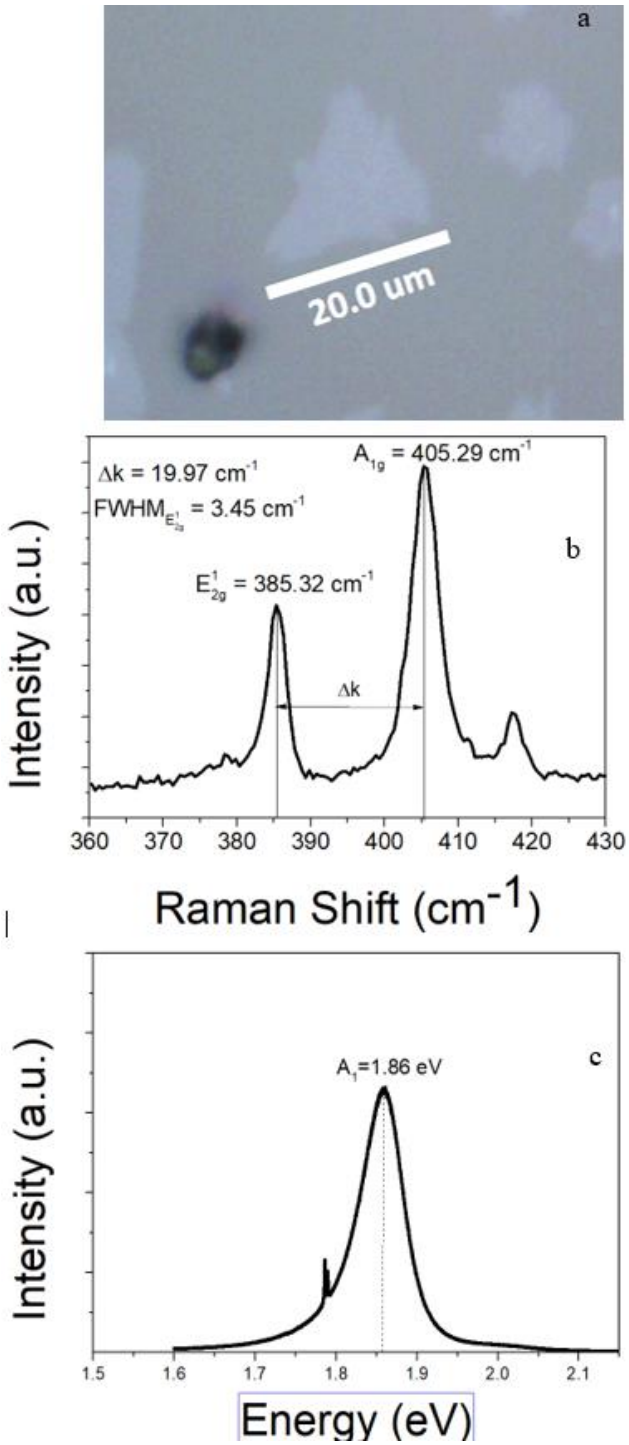

Figure 12. a) shows an Optical image of a MoS2 film growth in a Sapphire substrate using the process of Yi-Hsien, b) and c) are the Raman and PL Spectra of "a" confirming the film is Monolayer due to Raman ΔK of $19.97cm\hat{}-1$ and a strong A_1 in PL.

`

2.2.4 CVD and Seed Promoter (SiO_2)

The use of seed promoters has probed a high efficiency in MoS_2 CVD growth, crystallographic structures has been used reduced graphene oxide and perylene-3,4,9,10-tetracarboxylic acid tetra-potassium salt (PTAS) this is supported by Xi Ling [39]. This is due to the affinity of nucleations to grow in rough surfaces, adding this kind of seed promoters to the bare substrate (after cleaning processes) creates a controllable environment for the MoS_2 to growth. Furthermore, another reason to use Seed Promoters is that they avoid layer over layer nucleation, making a large are MoS_2 Film instead of just short islands of MoS_2. The results obtained in this work are shown in Figure 13.

For this experiment it was followed the recipe of Xi Ling process [39], which consist of preparing a solution of 50µM of PTAS in DI water, then by drop casting coat the substrate and then let the solution evaporates inside a fume hood for about 10 mins, once evaporated it is important to anneal the sample in a vacuum tube at 200˚C for half an hour to make sure there is not solution residuals on it, just the PTAS particles. After that this substrate can be used as a regular substrate for the CVD process mentioned before. The process is showed in figure 13.

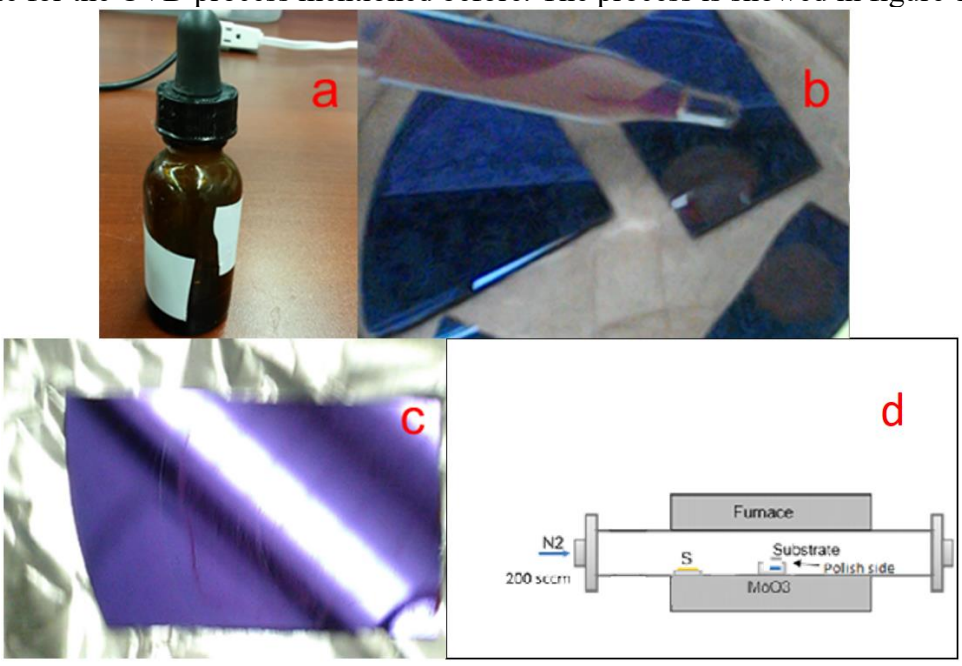

Figure 13. PTAS addition proces, a) solution of %0um PTAS in water, b) drop casting substrates, c) annealing, d) use the substrate as a regular CVD process, image obtained from reference [40].

`

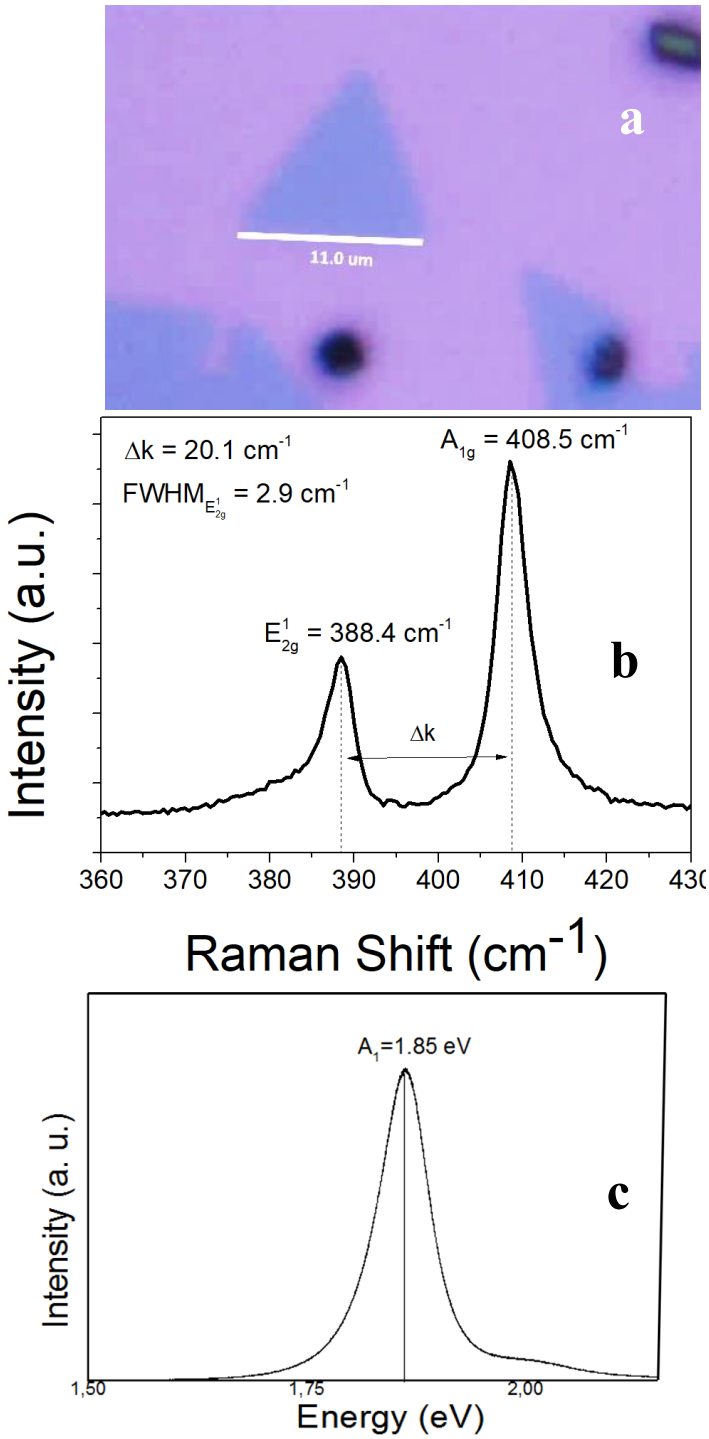

Figure 14. image a) shows a monolayer Flake of MoS_2 of around 11.9um per side, the spectrums in b) and c) are Raman and PL respectively, which confirms the flake in "a" is monolayer due to a ΔK around 20.1cm^-1 in Raman and a Strong A_1 peak for PL.

`

2.3 Comparison of Raman and Photoluminescence Spectra for MoS_2 Mech Exfoliated And CVD (SiO_2, Sapphire And SiO_2 with PTAS)

For MoS_2 There are 3 typical indicators in the peaks from bulk to monolayer [22]. First, the more the number of layers in the peak E_{2g}^1 will exhibit a regularly blue shifted while A_{1g} will show an opposite red-shifted broadening the frequency distance ΔK. Second, E_{2g}^1 and A_{1g} are located at approximately 387.0 cm^{-1} and 406.9 cm^{-1} for single layer MoS_2. Third, the peak frequency difference between E_{2g}^1 and A_{1g} shows a clear decreasing trend as a function of number of layers, meaning that the shorter the peak frequency the less the number of layers being around $19cm^{-1}$ for Monolayer flakes of MoS_2 and above $25cm^1$ for bulk. Figure 12 is a visual comparison between Raman spectra from MoS_2 films obtained by Mechanical exfoliation, CVD on SiO, CVD on SiO_2 aided by seed promoter, as well as CVD on Sapphire.

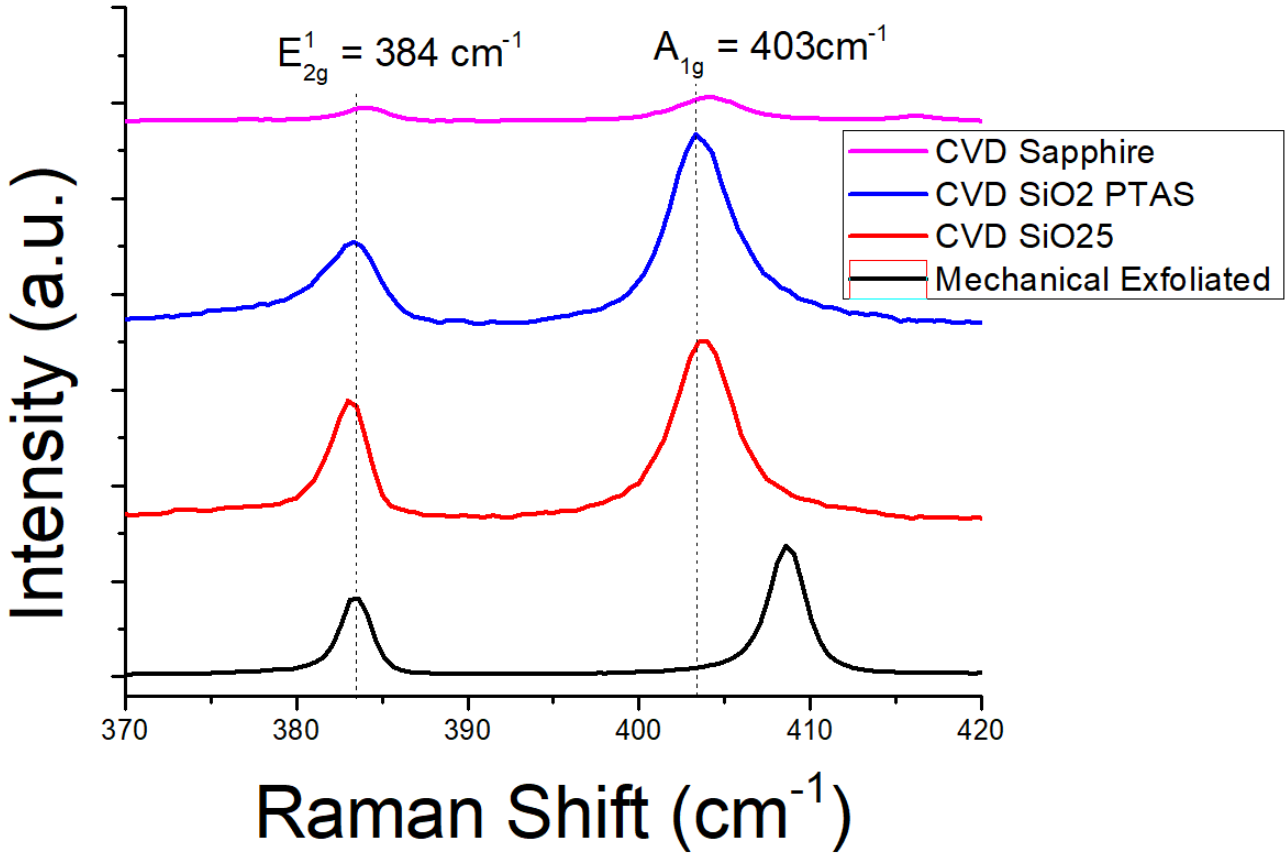

Figure 15. Raman spectra from the different synthesis methods used in this work. the black line corresponds to the Mechanical Exfoliated MoS_2 Few layer, the red line is the Raman spectra from the CVD MoS_2 Single Layer, the blue line corresponds to PTAS aided CVD MoS_2 and finally the pink line corresponds to the CVD MoS_2 on Sapphire substrate. The dotted lines are set at the characteristic raman peaks E^1_{2g} and A_{1g} at 384 cm^{-1} and 403 cm^{-1} respectivelly, acording to the literature[11].

`

CHAPTER 3: MOS_2 PHOTODETECTOR FABRICATION

3.1 Fundamentals of Photodetector Fabrication

In this chapter some background is introduced, starting from the definition and classification of the different photodetector configurations. After that some basics of physics that rules the functionality of photodiodes are explained in order to get an overall which will help to understand the device performance that will be in next chapter. Finally, the fabrication process used in this work will be explained and supported by optical images. Two basic photodetectors were built, the first one is a basic MoS_2 Mechanical exfoliated photodetector (Bottom contacted with Mo) made by viscoelastic stamping method. And the second one is a MoS_2 CVD synthetized photodetector (top contacted with AL). the MoS_2 Mechanical exfoliated photodetector was coated with Au nanoparticles in order to achieve the Surface plasmon effect, the performance of this device will be presented in the next chapter.

3.2 Photodetectors classification

Photodetectors are described as photoelectronic device that are able to absorb optical energy from the electromagnetic spectrum and convert it to electrical energy[41], which usually is known as photocurrent. An ideal photodetector might fulfill the requirements of having high sensitivity, low noise, wide bandwidth, high reliability and low cost. The flagship of photodetectors are photodiodes when photons are absorbed in the metal surface they create electron-hole pairs (aka exciton pairs) in the depletion region, once charge carriers are produced in the semiconductor material the carriers reach the junction by diffusion.

Another type of photodetector is the PIN Photodiode; a regular photo diode configuration that includes an intrinsic layer between the P and N type materials. PIN is only reversed bias configurated due to the high resistivity of the intrinsic layer. PIN has larger depletion region which allow more e-h pairs to be created at lower capacitance. PIN diodes have better frequency response due to electron mobility greater than hole mobility. PIN also has larger breakdown voltage in

comparison with PN diodes, this allow them to be used with a biases voltage of approx. 100, which make the time response faster[42].

Avalanche Photodiode is another type of photodetectors, that works close to the breakdown voltage which cause photoexcited carriers to accelerate in the depletion region and produce additional carriers by an effect called avalanching[42]. This type of diodes is good for fiber optic systems that require additional low light levels with Q. Efficiency larger than 100%. Finally, the Phototransistor; since it is configured as PNP or NPN it can be said that Phototransistors have a photodiode with an internal gain. Phototransistors are represented by a bipolar transistor that is enclosed in a transparent case so that the photons can reach the base-collector junction. The electros generated by photons in the base-collector junction are injected into the base and the current is then amplified[42]. Phototransistors can't detect light any better than photodiodes since they are in the same range. The drawback of a phototransistor is the slower response time in comparison to a photodiode, it is only different configuration as we can see in the image bellow. A schematic of a photodiode and a phototransistor is shown in figure 15.

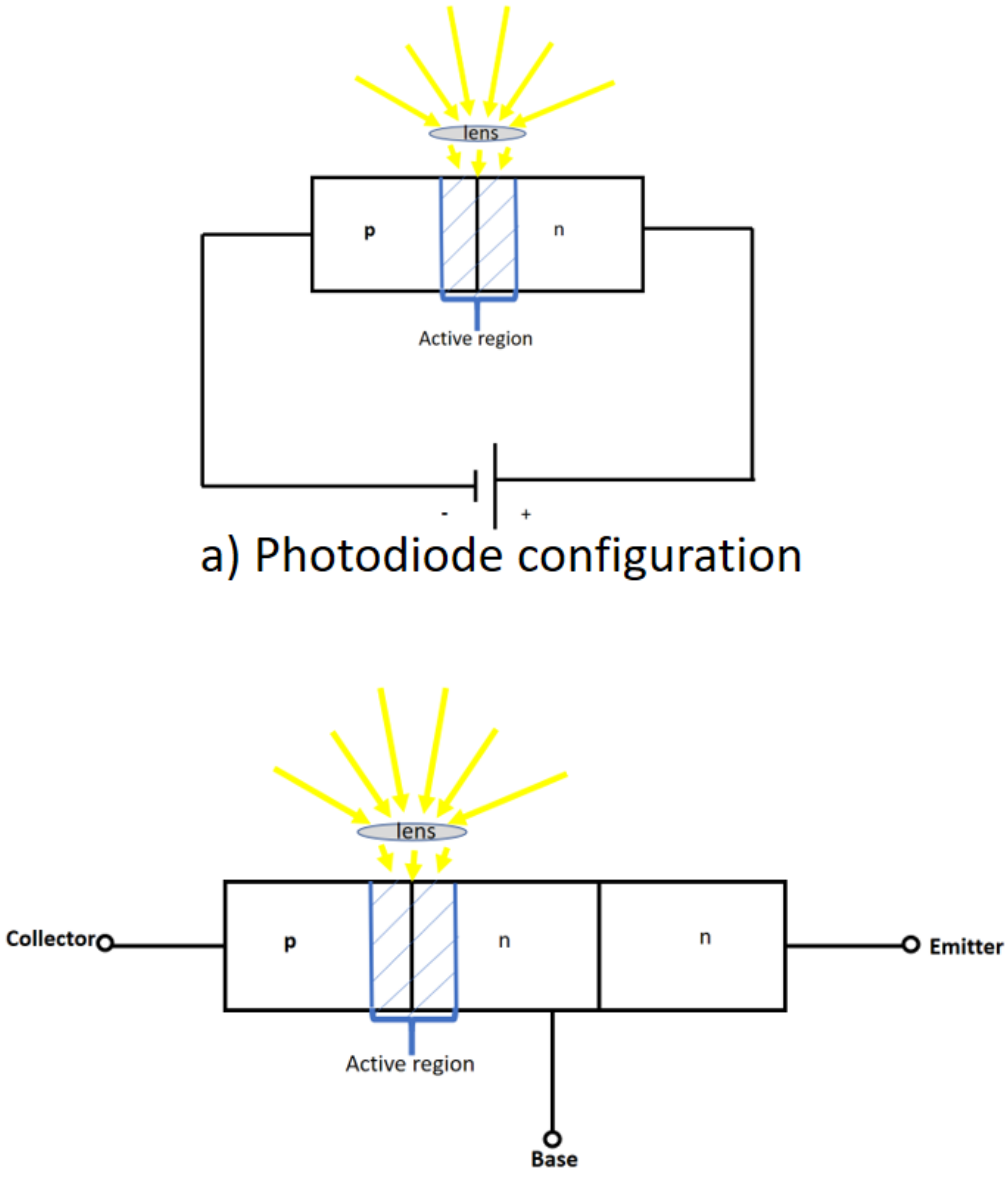

Figure 16. schematic of two different configurations of photodetectors, a) photodiode and b) phototransistor. The purpose of this image is to understand why no matter how complex can be a phototransistor the performance will be the same as a photodiode or even lower because phototransistor configuration can be seen as two photodiodes but the effective area where the light creates the exciton pair is only one.

`

3.3 MoS_2 Photodetector Fabrication Methods and Results

3.3.1 Introduction

in this section the main idea is to explain the fabrication methods performed in order to build the photodetectors presented in this work. The devices are basically two MoS_2 based photodiodes made of different processes, the first one is a Mechanical exfoliated (bottom contacted with Molybdenum). And the second one is a photodiode made of MoS_2 CVD Synthetized (top contacted with Aluminum). Moreover, to study the effect of the surface plasmon resonance the Mechanical exfoliated flake will be covered with Gold (Au) nanoparticles. Optical and electrical Characterization techniques were performed on this device before and after the Au nanoparticles coating, in order to compare the results and be able to identify an improvement.

3.3.2 MoS_2 CVD Synthetized Photodetector

The first fabrication method presented in this work is a MoS_2 CVD Synthetized Photodetector, which is classified as a Top-contact photodetector. The process started with a MoS_2 film Few-layer obtained by CVD synthesis using the process mentioned in Chapter 2. After having identified the film to be used, some characterization techniques such as Raman Spectroscopy and Photoluminescence were performed in order to make sure the material is MoS_2 as well as to be able to know how many layers does this film have with respect the number distance between peaks[11]. For this experiment figure17 image a) shows the MoS_2 film about 4 layers according to delta K in Raman shown in figure image b) meanwhile image c is the photoluminescence of MoS2 in a)

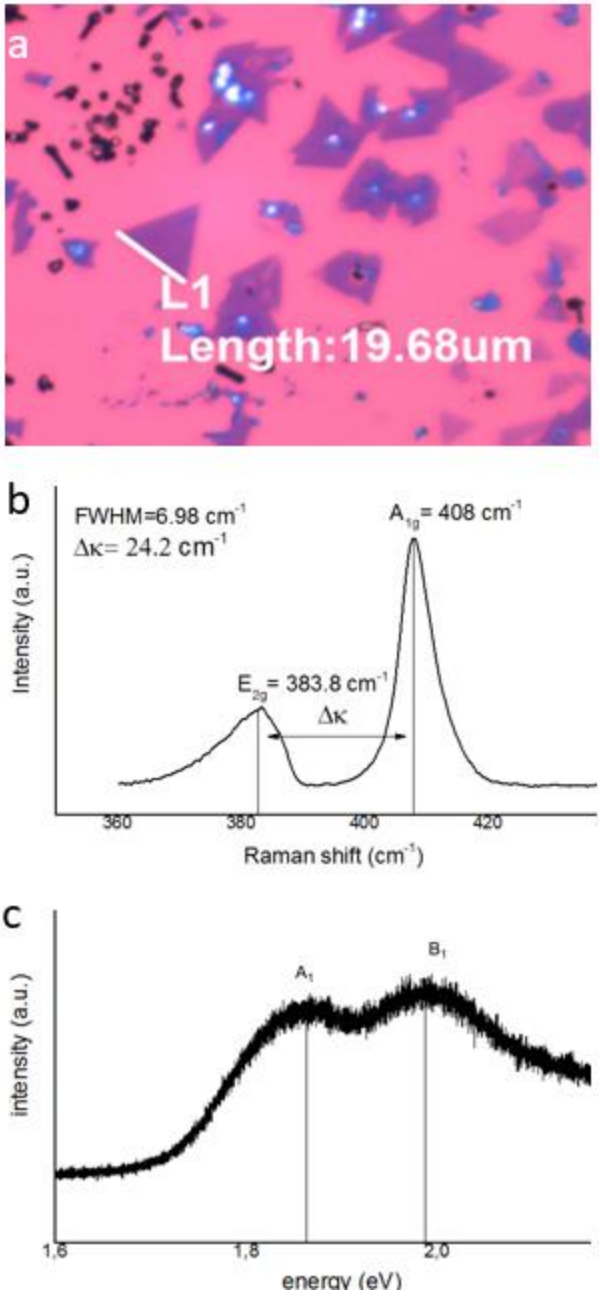

Figure 17. a) Optical image of MoS2 4L Mag x100 , b) Raman before contacts deposition, c)) PL before contacts deposition,

`

Then, it is needed to put some metal contacts on it to create the metal-semiconductor junction which will give us the effective area for developing the Photodetector. In order to get a good shape and very well-defined contacts a photolithography process is utilized to make the pattern on the sample, this pattern allows to define the shape of the contacts, for this experiment it was utilized the photolithography method explained in 3.3.

Finally, the metal contact deposition was developed by using a CHA SE-600 Electron Beam Evaporator shown in figure 19. This process will be explained in detail in 3.3.3.3, some images of the results are shown in figure 18, as well as a Raman spectroscopy after the metal deposition in order to be able how the metal contact affect the behavior of Raman Scattering.

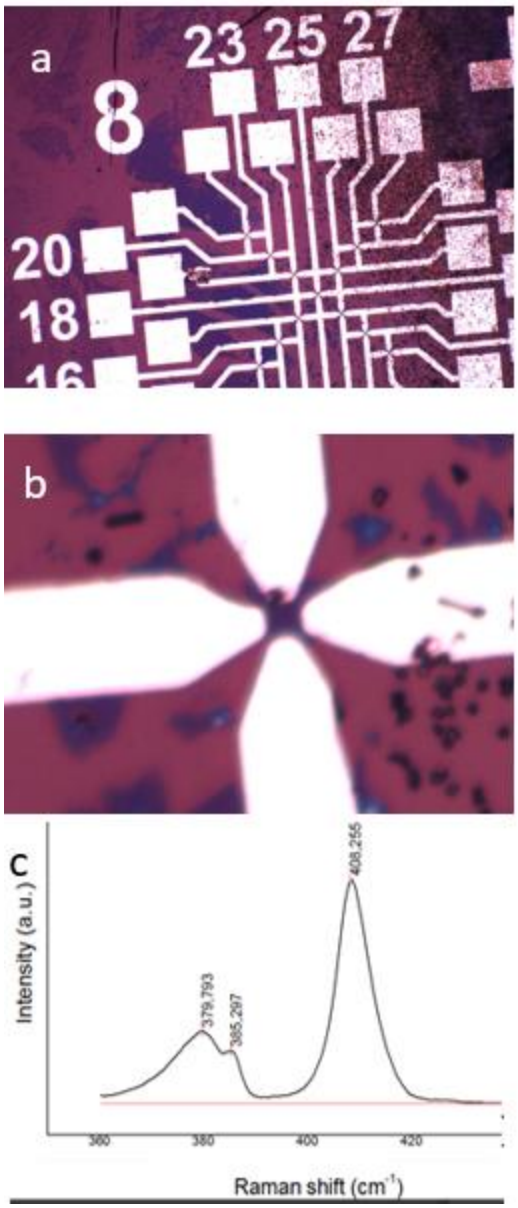

Figure 18. a) Optical image of MoS2 4L with Aluminum contacts deposited by e-beam evaporator, Mag x10, b) MoS2 4L with Aluminum contacts deposited by E beam evaporator, Mag 50X, c) Raman after contacts deposition

`

3.3.2.1 Transfer Process basis for flexible electronics

MoS2 is a suitable material for developing flexible or bendable material due to its mechanical properties mentioned in Chapter 1 like high strength and yield. However, temperature conditions in CVD synthetized is a limitation for using flexible substrates directly because most of these materials are polymers which happens to have low fusion point and in consequence polymer gaseous particles will be interacting during the MoS_2 synthesis process, which could affect the reaction between precursors. Therefore, it is necessary to implement a transfer method for CVD synthetized MoS_2 to be able to develop flexible electronics which allows to keep the quality of the TMDC film after the transference process.

Currently, the most used transfer method is the process developed by K. M. McCreary which is a wet processing method that involves SiO_2 etching with hydrofluoric acid (HF) solution [43]. By using this method, it is possible to make the transfer, keeping a good quality on the transferred material. However, the chemicals used in this method are environmentally harmful and involves potential risk in the process. The method starts by coating the sample with Poly-Methyl methacrylate (PMMA) using a spin coater, and then bake the sample for 5 minutes at 180˚C. later the sample is submerged in a plastic container with HF based solution, for this experiment it was used Buffered Oxide Etchant (BOE). After approximately thirty minutes some bubbles can be seen at the edges of the sample, the sample can be taken out after many bubbles can be seen between the sample and the PMMA film, this depends on the sample size as well as the concentration of the solution used. some results of this process are shown in figure 19.

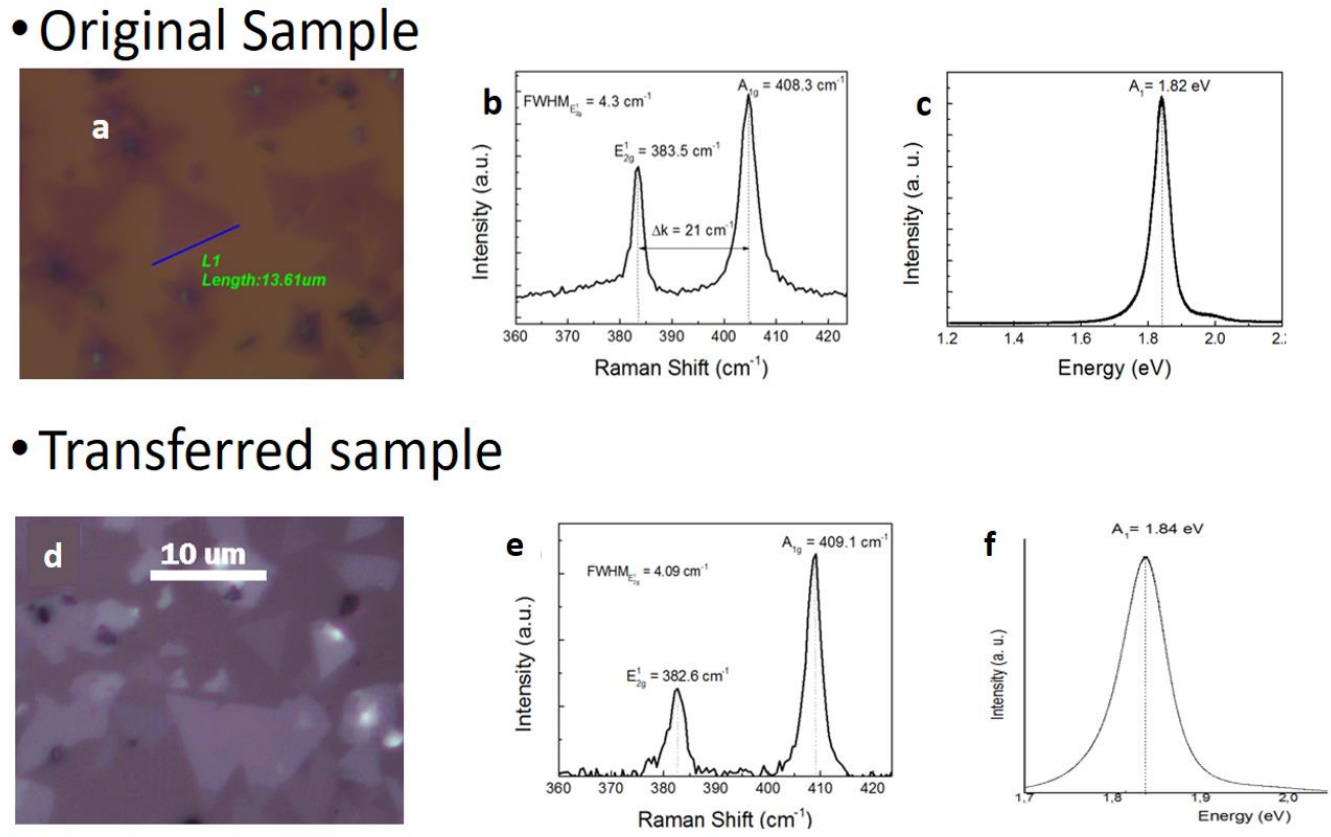

Figure 19. a) Optical image of MoS2 Monolayer transferred to an SiO2 50x, b) Raman of flake in fig "a", d) PL of flake in fig "a", d) Optical image of MoS2 Monolayer transferred to a Polyamide substrate 50x, e) PL of flake in fig "a", f) Raman of flake in fig "a", d) PL of flake in fig "a".

Some alternatives were studied, such as the etching free transfer method developed by D. Ma. This method is more ecofriendly and eliminates the hazardous materials usage. The transfer method D. Ma. proposes uses only DI water and sonication bath as a mechanism of transfer, which is possible by taking advantage of the weak Van der Walls forces of the MoS_2.[44] However, this method has the inconvenience of a decrease in the quality of MoS_2 transferred; due to sonication mechanism the MoS2 domains can be broken and therefore the yield is reduced. In this work both processes were performed in order to compare the results which contribute to continue with the Flexible photodetector development, some results are shown in figure 20. Nevertheless, the metal contact deposition for polymers is a pendent work

`

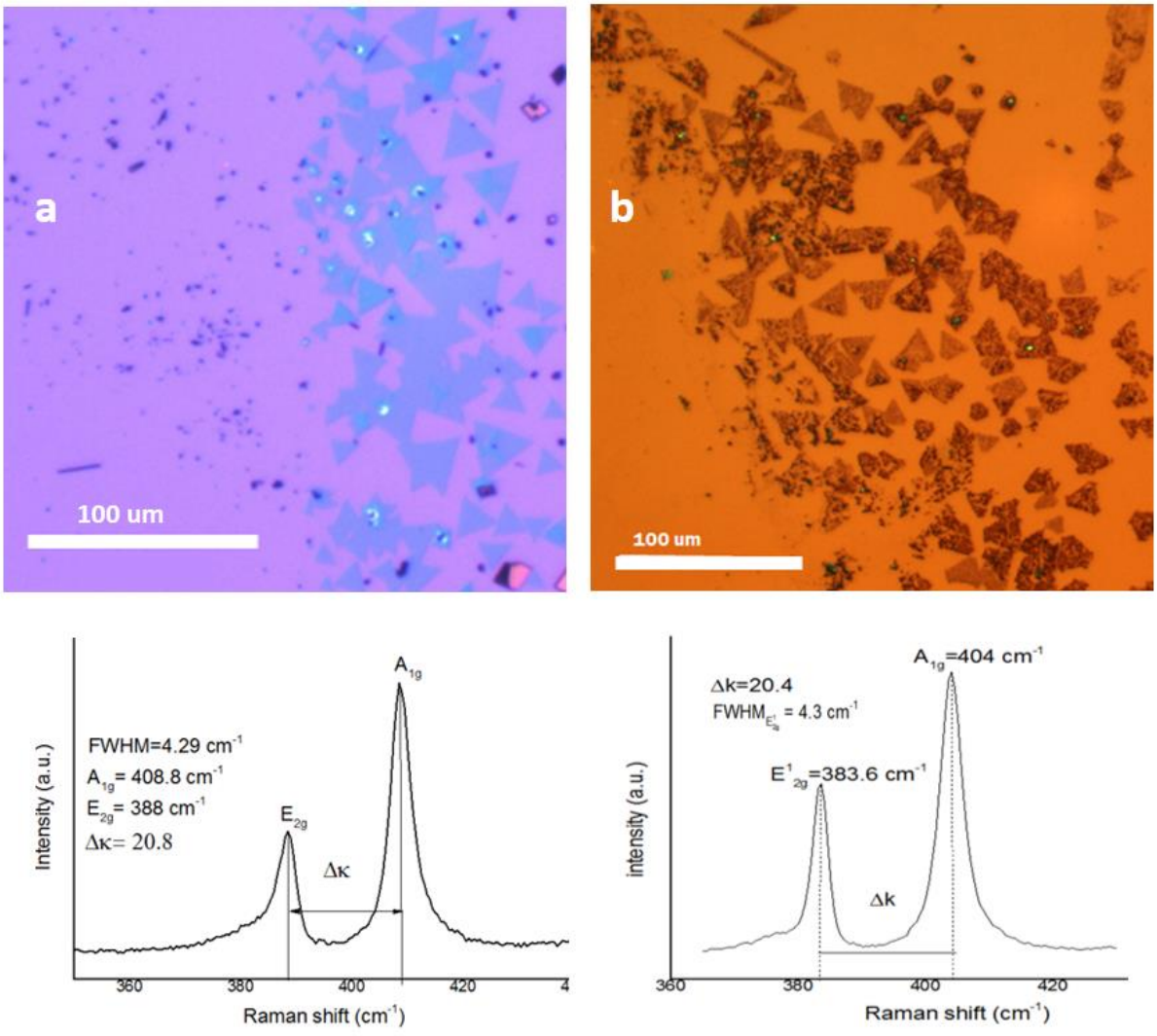

Figure 20. a) Optical Image of MoS2 CVD synthetized b)Optical image of MoS2 Monolayer after transferred to an SiO2 by water sonication method, c) Raman of flake in image "a", d) Raman of flake in image "b".

`

3.3.3Mechanical Exfoliated MoS2 Photodetectors (Metallic Bottom contacts)

3.3.3.1 Introduction to Fabrication of a Mechanical Exfoliated MoS_2 Photodetector

Mechanical exfoliation is considered to be the method with the highest quality in MoS_2 films obtained, due to it is a process that starts from the pure crystal and does not involve any chemical processes. For this fabrication process we will be using a MoS_2 sheet obtained by Mechanical exfoliation, this method was already explained in chapter 2 section 2.1.

In this work it has been developed a Photodetector by using a Mechanical Exfoliated MoS_2 film and metal contacts made of Molybdenum. This device is bottom contact since the MoS_2 film is placed on top of Mo contacts creating a Metal-Semiconductor-Metal Junction which leads to a Schottky contact. The method is described below.

3.3.3.2 Metal Contact Deposition on Silicon Dioxide (SiO_2)

Since this is a Metallic bottom contact configuration, it is needed to deposit metal contacts in a Silicon Wafer previous to the addition of the MoS_2 film. The parameters to take in consideration when building a FET or photodetector made of a 2D TMDC is the type of behavior of the film, since 2D TMDCs has natural direct band gap they behave as a n or p type, for MoS_2 it is usually reported to have a n-type semiconductor behavior [45]. The parameters to be considered for making a photodiode made of TMDCs monolayer are: the material for the contact which will be responsible for the type of contact (either Schottky or Ohmic), usually the minimum Schottky barrier height is desired. This parameter can be obtained from the equation:

$$\varphi_B \approx \varphi_m - X \tag{2}$$

`

For the purposes of this work the Metal chosen was Molybdenum which has a work function about 4.33eV [46]. These Mo contacts will provide a Schottky contact (Metal-semiconductor-metal) and at the same time they work as protection for the thin film avoiding possible scratches from the probes.

One of the most important process on fabrication of devices is the patterning. The main purpose of this step is to create a specific shape with very well defined edges that will help to guide the metal deposition. For such a scale of integration this is achieved by using a photolithography method which by definition is a way to print an image over a surface by using light. This process needs a coat of a photo resin, a light source (UV-light), a crystal mask with the desired pattern, and an etchant to get rid of the residuals of resin.

In this experiment, the lithography pattern is reached by using lithography a mask of 150um squares for the pad contact and transmission lines of about 20um thick. The pattern consist of an eight-contact arranged in a circle way due to some 2D materials exhibit an anisotropic electrical transport or optoelectrical behavior, to prevent this, the eight contacts disposed in a circular way will contribute to be able to measure different angles[40]. The pattern was created by Gustavo A. Lara Saenz, an schematic is shown in figure 17.

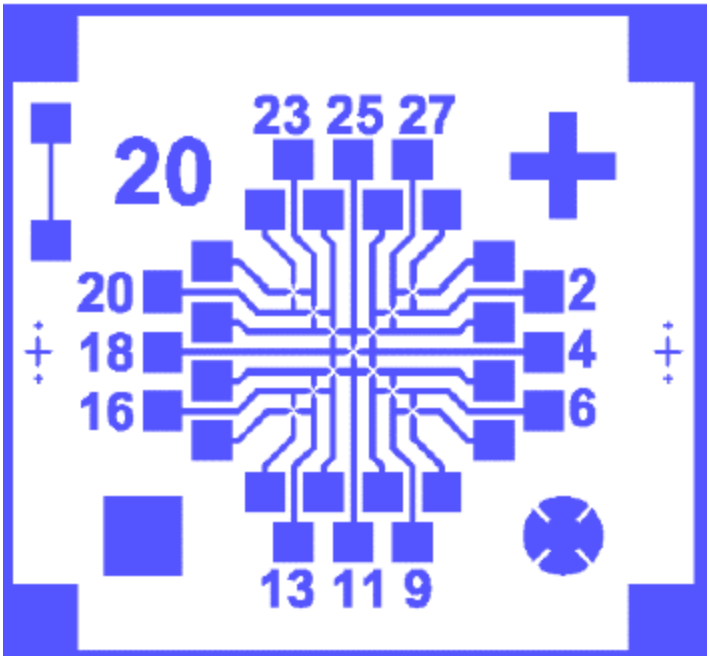

Figure 21. image obtained from Synthesis and Device Fabrication of two-dimensional molybdenum disulfide by Gustavo A. Lara Saenz [40]. showing the pattern in the lithography mask that was used for metal deposition. On blue color is the contact shape, this portion will be transparent, which means light will get through this shape hitting the photo resin. The white part is the covered part, this area will block the light, meaning this area will not be exposed by light.

In this experiment it was used Molybdenum (Mo) contacts patterned in a silicon wafer using a Photolithographic process described below, Figure 18 shows the final outcome of the wafer patterned with photoresist:

1st. Substrate cleaning; a270nm SiO_2/Si wafer is cleaned by using the Regular solvent process mentioned before in chapter 2, which consist of Acetone, Methanol, and DI water consecutively on sonication bath to remove all the oils and organic residues from the surface of the wafer.

2nd. Hexamethyldisilane (HMDS) layer deposition; this will serve as adhesion layer for the photoresist. First the wafer needs to be dehydrated on a hotplate at 150˚C for 4 minutes, after cooling, by drop casting HMDS will be poured all over the wafer surface, and then it will be

sonicated using the rate of 700rpm/5seconds, 4000rpm/40seconds, 500rpm/10seconds. Then bake on a hotplate at 110˚C for 2minutes, and let it cool down.

3rd. Photoresist coating; drop cast Az5214E-IR photoresist all over the surface of the wafer, then spin coat using the rate of 700rpm/5seconds, 4000rpm/40seconds, 500rpm/10seconds. Then bake on a hotplate at 10˚C for 1minute, and let it cool down.

4th UV exposure; using a Karl Suss MJB 3 UV 400, the photolithography mask is aligned over the silicon wafer with photoresist, the exposure time is 35 second with an intensity about 2mW/cm2.

5th Developing; this process must be done right after exposure, and consist on immerge sample in AZ300 MIF Developer during 30 seconds then wash twice with water and dry with N2.

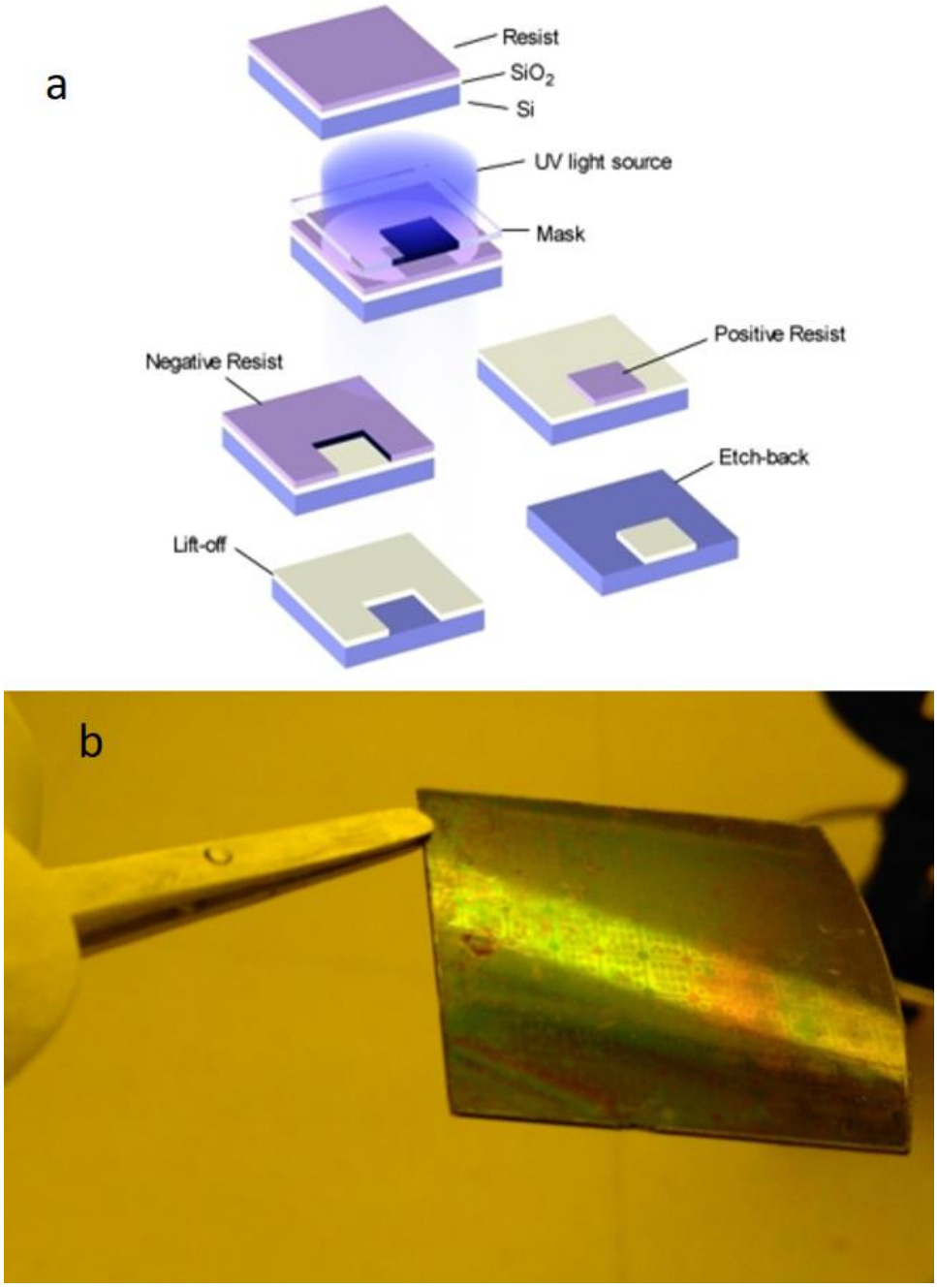

Figure 22. image a) obtained from [47], shows the principle of photolithography, b) is a picture of the results gotten in this work by using positive resist.

`

3.3.3.3 Metal deposition

The deposition of the metal contacts was achieved by using a Physic Vapor Deposition (PVD) technique. This process is carried out on a "CHA SE-600 Electron Beam Evaporator with Cryopump" shown in figure where highly energized argon ions are bombarded to the targeted Molybdenum pellet. This process releases particles from the Molybdenum that will be deposited on the silicon wafer inside the chamber, the hole process is made under high vacuum conditions to avoid contaminations. The deposition parameters were 3 mTorrs of pressure and 200W of DC power for 20 minutes, which will give us as a result a Mo layer of 200nm thick.

Some captions and the thickness profile obtained by using a profilometer Bruker Dektak XT are presented in figure 19, where it can be seen that the average point in height for pads and tracks are around 200nm.

Figure 23. CHA SE-600 Electron Beam Evaporator with Cryopump used to deposit metal contacts. The basis of this process consists of apply a current through a tungsten filament which leads to joule heating and electron emission, then a strong magnetic field focuses the electrons into a unified beam which is directed to the deposition material (Mo in this case) causing it to evaporate and deposit onto the substrate.

`

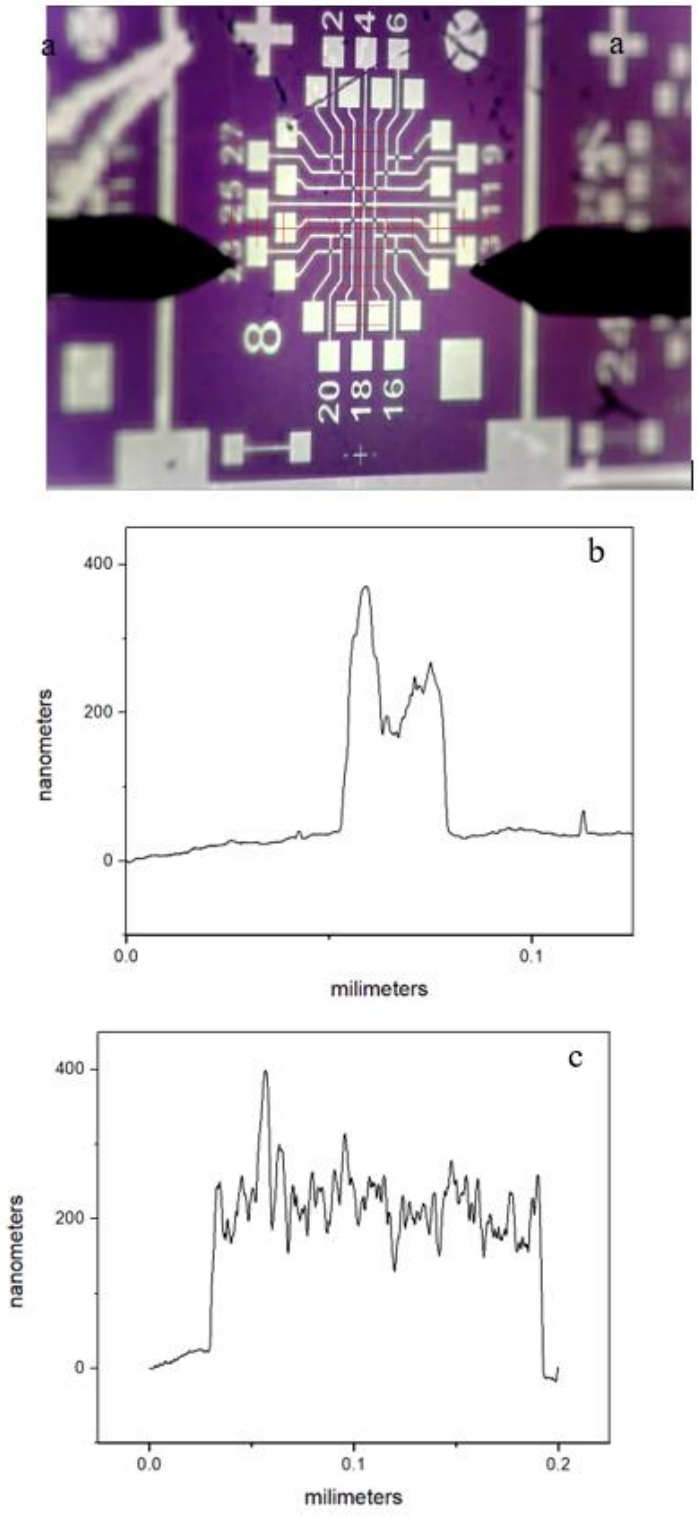

Figure 24. a) is an optical image of the metal contact deposited under the profilometer microscope, b) shows the trace thickness and c) shows the thickness of the pad.

`

3.3.2.3 Viscoelastic Stamping

In this section it is presented Andre's Castellanos method [48], this is a very straightforward method for transfer Mechanical Exfoliated Films from one substrate to another one taking advantage of the weakly van der Waals forces in the out of plane regime. This is a very trustable method and it is very cheap as well. In this process it was utilized a mask aligner Karl Suss MJB3 shown in Figure 20. for the alignment and transference.

Figure 25. picture of the mask aligner Karl Suss MJB3. Used to perform viscoelastic stamping.

`

Basically, the main purpose of this method is to use a transparent gel-film (PDMS) which is adhered in a 4'X4'glass. Which corresponds to the dimension for mask holder in mask aligner. Then the substrate with the Mo contacts is held by double coated carbon tab on the substrate chuck and the glass positioned in the mask aligner. The transfer is achieved by using the microscope and micromanipulators of the mask aligner. Some pictures of the process under the microscope are shown in Figure

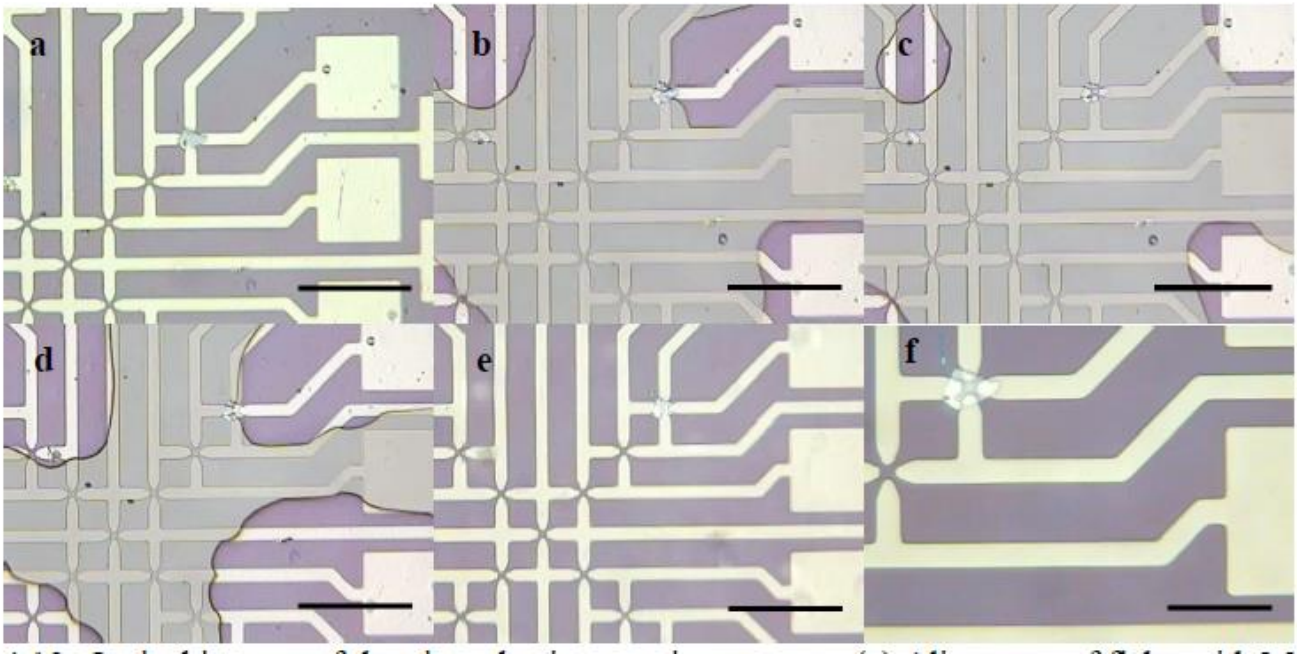

Figure 26. Viscoelastic stamping process under the microscope, picture obtained from "Synthesis, Device Fabrication And Characterization Oftwo-Dimensional Molybdenum Disulfide by Gustavo Alberto Lara Saenz [40] (a) is the alignment of the MoS_2 film, (b) deformation of the gel due to pressure applied for the chuck of the mask aligner, (c) flake completely in contact with substrate, (d) gel removal, (a) and (f) shows the MoS_2 film transferred onto the substrate with Mo contacts.

In summary a photodetector was fabricated with mechanically exfoliated MoS_2 flake using viscoelastic stamping mentioned [12]. The photodetector consists in bottom Mo contacts with a channel length of 12 μm, a channel width of 20 μm, and a MoS_2 area of 1780 μm^2. The fabrication process was executed as follow. First, the contacts were fabricated by standard photolithography process using AZ 5214-IR photoresists, followed by Mo deposition via sputtering in 3 mTorr of

`

Ar ambient at 200 Watts of power, and lift-off with acetone. Afterwards, the MoS_2 was exfoliated and transferred to PDMS film and aligned, and placed in contact with the target substrate using the mask aligner Karl Suss MJB-3, taking advantage of the microscope and micromanipulators. The optoelectronic measurements of our device are shown in next chapter.

3.3.3 Plasmonic Effect and Au Nanoparticles

3.3.3.1 introduction

By definition, plasmonic oscillations of free electrons at metal-dielectric interfaces or boundaries are referred to as surface plasmon resonances, which support intense electromagnetic (EM) field concentrations which are tailored to confinement the incident optical power in subwavelength dimensions at the optical frequencies [49]. This is carried out by a hybrid particle called surface plasmon polarization (SPP) created by the excitation of surface plasmons with light. this hybrid particle SPP is composed of charge oscillations coupled to EM waves, which means that they are created from light by the coupling of photons on the conduction electrons in small subwavelength metal nanoparticles.

Plasmonic resonance can improve the efficiency in photodetectors by 3 ways; pronounced optical absorption, field localization, and scattering effects. This phenomenon causes a large electromagnetic field enhancement which takes place in the vicinity of the metal surface and the dependence of the plasmon resonance wavelength on nanostructure size, shape and local dielectric environment, or form very strong scattering effects that occur at wavelengths in the vicinity of plasmonic resonances[50].

Periodic arrangement of scattering structures at the top of the device can enable large enhancement in photocurrent response at specific wavelengths [51]. therefore, periodic

arrangements of metallic structures cause a photocurrent response enhancement, enabling large wavelength-specific increments in photocurrent.

Radiative modes are energetic SSP that are above the ω_p, which are above the light (i.e. Silver ω_p=3.9eV), in this regime, radiative bulk plasmon modes are observed and the metal behaves like a dielectric and the dielectric function of the metal is positive. Therefore, light with large wave vectors can excite characteristic surface plasmon frequencies ω_p around 3.7eV.

3.3.3.2 Grating-Coupled plasmonic photodetectors

Grating-Coupled plasmonic photodetectors is a kind structure widely used in plasmonic detectors for momentum mismatch between the incident light and the SPPs, the major advantage of this structure is easy fabrication and integration could be realized simply by depositing comb-type metallic parts on a multilayer semiconductor [52]. Using this kind of structure is possible to compensate momentum by supplying additional momentum to the incident light caused by the periodicity of the grating because this structure allows to excite SPP when light is incident from above or below the grating

3.3.3.2 Experimental procedure

For this experiment it was used the Mechanical Exfoliated photodiode previously fabricated, and Gold nanoparticles of 15nm diameter from Sigma Aldrich, this is a stabilized suspension in 0.1mM Phosphate Buffered Saline (PBS) reactant free in Figure 22 is presented the absorption spectra of the Gold Nanoparticles 15nm diameter. Electrical characterization of the Mechanical Exfoliated MoS_2 Photodetector was measured before and after adding the Au nanoparticles, such characterization results are shown in chapter 4.

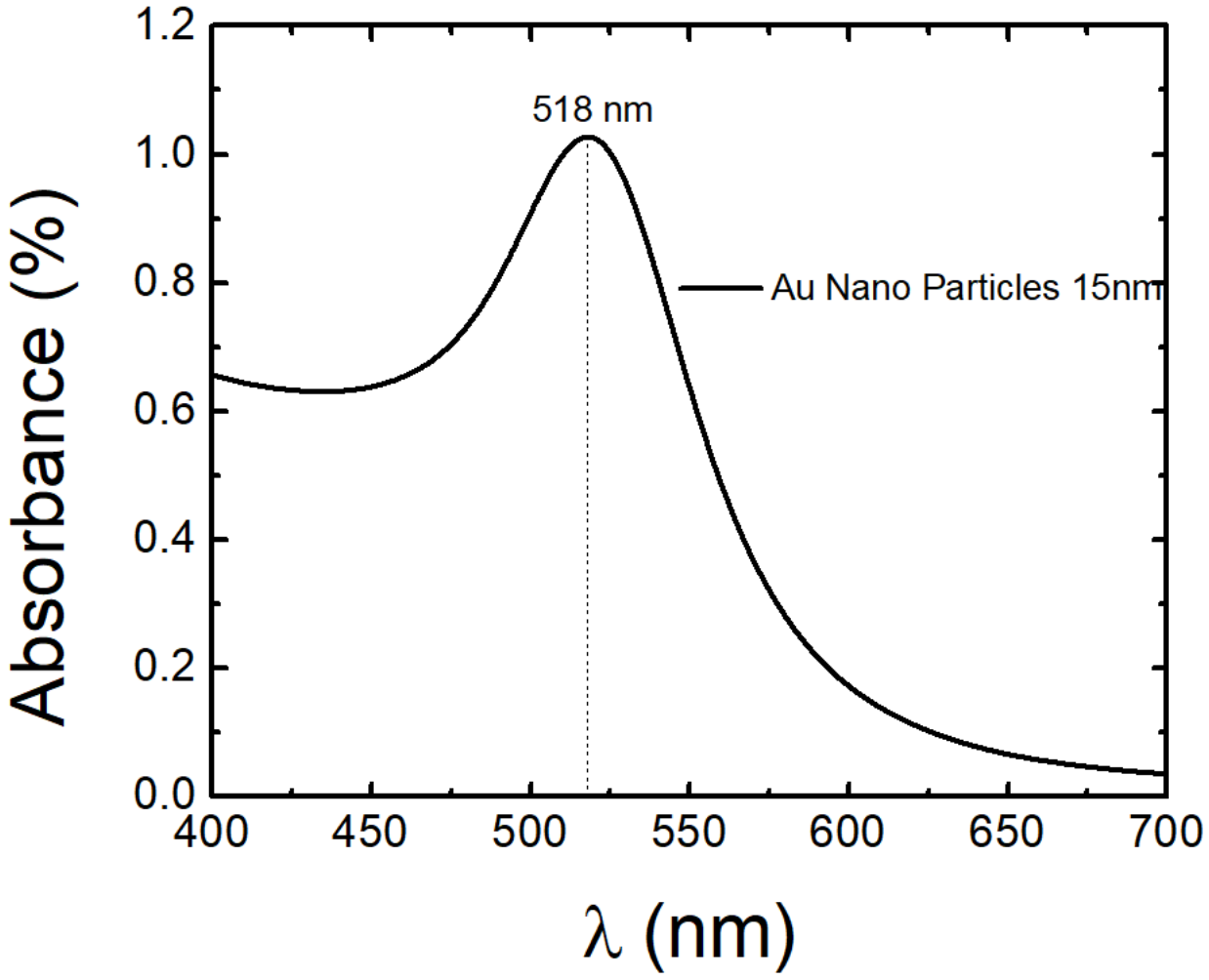

Figure 27.Absorbance of 15nm Diameter Au nanoparticles, performed by using a Cary UV-vis spectroscope, showing an absorbance of around 518nm.

For being able to see the plasmonic effect it is needed to use one of the structures mentioned in the article "Plasmonics for improved photovoltaic devices" [16]. For the purposes of this work it was used the light trapping by scattering from metal nanoparticles at the surface of the photodetector shown in Figure 24. By using this configuration light will be scattered and trapped into the semiconductor thin film by multiple and high-angle scattering, allowing an increment in the effective optical path length in the photodetector.

`

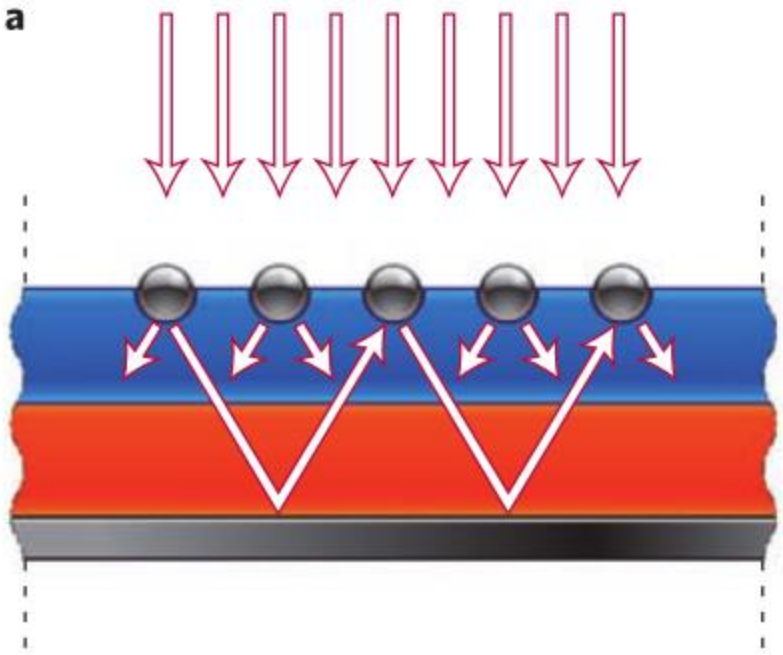

Figure 28. image a) is an schematic of a light trapping by scattering from metal nanoparticles at the surface of the photodetector, image obtained from[16].

To achieve this structure configuration, the Mechanical Exfoliated MoS2 Photodetector previously fabricated was coated with the 14nm Au nanoparticles by drop casting 1um of the Au nanoparticles in PBS solution, over the surface of the MoS_2 film in the Photodetector. In order to get rid of the solvent the sample was annealed up to 200˚C in a vacuum evaporator for about 40 minutes. Images of before and after Au nanoparticles are presented in figure 25. After that the photodetector was electrically characterized in a lakeshore crx-4k probe stage again in order to compare the measurements before and after Plasmonic effect.

`

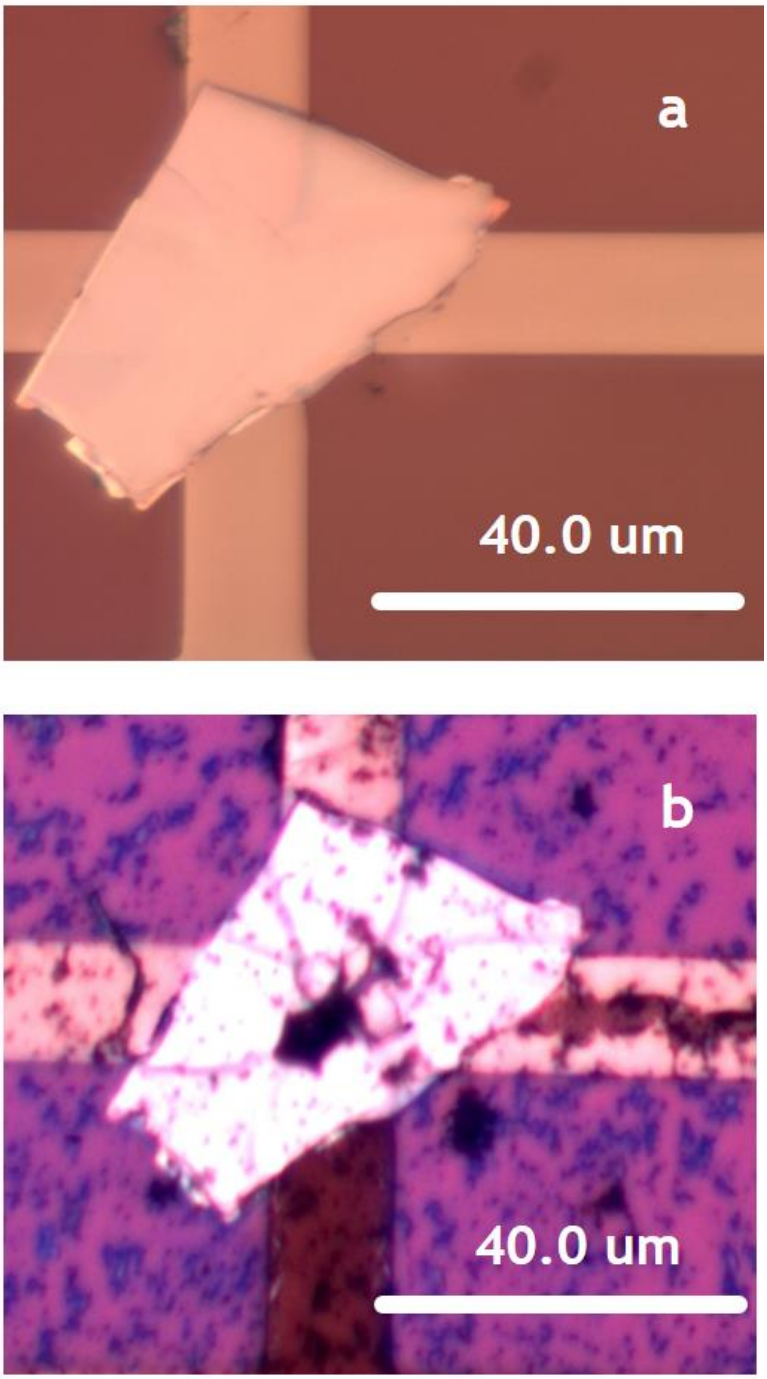

Figure 29. optical images 50X Magnification, a) shows the Mechanical exfoliated MoS_2 before Au nanoparticles coating, b) shows the same device after adding Au nanoparticles.

`

CHAPTER 4: OPTICAL AND ELECTRICAL CHARACTERIZATION

4.1 Fundamentals of Photodetectors

In order to understand the functionality and the way to improve a photodetector is Important to keep in mind some definitions. As we mentioned before, there are two possible photodetection mechanisms.

The first one is related electron-hole pairs generation (EHP); carried out on the semiconductor surface caused by absorption of photons from an optical power source of energy, where this energy is greater than the bandgap energy of silicon ($E_g = hv$)[19], this kind of generation has three fundamental steps:

1st the incoming optical power is absorbed by the semiconductor and leads to creation of EHP
2nd The applied reverse bias $V_b<0$ to the Schottky metal contact, forms a depletion region with high electric field which causes the EHPs to be separated and carried across the absorption area
3rd the photocurrent is formed by collection the EHP at the device contacts.

Other possible mechanism is based on the creation of hot carriers in the metal, via internal photoemission process (IPE)[19], in this mechanism the energy of the incoming light must be greater than the Schottky barrier energy. This process can also be described by 3 steps:
1st the absorption of light by metallic parts leading to the photoexcitation of hot carriers
2nd hot carriers are transported to the Schottky contact
3rd the emission and collection of hot carriers over the Schottky barrier into the semiconductor under applied reverse bias producing photocurrent

Bellow some physical phenomena driving photodetection are described[53]:

4.1.2 Absorption Rate

Absorption Rate "R_{abs0}"; is the number of photons absorbed by the semiconductor per second per unit volume:

$$R_{abs} = \frac{P_{inc}}{hv} / V_v \tag{3}$$

4.1.3 Generation Rate

Generation Rate "G"; are the e-h pair created by the photon flux (Absorption Rate)

Acording to mass action law

Meanwhile Optical Recombination rate is given by

$$R \sim rnp \tag{4}$$

where r is a personality constant

The Generation rate is given by

$$G = rn_i^2 \tag{5}$$

At equilibrium Generation rate will be equal to Recombination:

$$G = R \tag{6}$$

Therefore

$$rn_i^2 = rnp$$

`

4.1.4 Internal Quantum Efficiency

Internal Quantum Efficiency "IQE"; is the ratio of generation rate "G" to the photon absorption rate, in other words is the ratio of the number of charge carriers collected by the photodetector to the number of photons of a given energy impinging in the effective area of a photodetector that are absorbed:

$$\eta_i = \frac{G}{R_{abs}} = \frac{GV_v}{P_{inc}} = \frac{G}{P_{inc\,1}} \tag{7}$$

where:$P_{inc}$is the total power absorbed in the sample, V_v = volume of semiconductor sample, and $P_{inc\,1}$ is the absorbed power density (cm^-3)

4.1.5 External Quantum Efficiency

External Quantum Efficiency "η"; is the number of carriers (electron-hole pairs) per second collected to produce the photocurrent divided by the number of incident photons per second:

$$I_{ph} = q\eta \frac{P_{inc}}{h\nu} \tag{8}$$

Solving for η and plugging Responsivity, External Quantum Efficiency can be seen as:

$$\eta = R\left(\frac{hc}{\lambda}\right)\frac{1}{q} \tag{9}$$

4.1.6 Responsivity

Responsivity "R" by definition is the ratio of energy in (watts) incident on the photodiode and the photocurrent output (Amperes) it is expressed in A/W and measures the input-output gain of a detector. Many common photodetectors respond linearly as a function of the incident power. Responsivity is given by:

`

$$R = \frac{I_{ph}}{P_{inc}} = \frac{\eta q}{h\nu} = \frac{n\lambda(\mu m)}{1.24} \quad (10)$$

With units in A/W

Primary Photocurrent; is the current passing through the photodetector (of any type) when all the photo-generated carriers are separated in the electric field and are swept out without replenishment

- If the generation "G" is uniform then: $I_{ph} = qG_V$ (11)
- If the Generation is not uniform: $I_{ph0} = qS\int_0^L G(x)dx$ (12)

where: L=Length, S=cross-section area of the sample

4.1.7 Photocurrent and Gain relation

Photocurrent may be greater or smaller in real devices, for various mechanisms increasing or decreasing actual photocurrent there is an addition factor called Gain.

- Gain in photoconductors Γ_G;

$$\Gamma_G = \frac{Path\ traveled\ by\ electron + path\ traveled\ by\ hole}{Length} \quad (13)$$

$$\Gamma_G = \frac{(\mu_e \frac{V}{L}\tau + \mu_h \frac{V}{L}\tau)}{L} = \frac{(\mu_e + \mu_h)}{\mu_e} \frac{\tau}{\frac{L^2}{\mu_e V}} \quad (14)$$

Where: τ is the electron and hole lifetime and $\frac{L^2}{\mu_e V}$ = electron transit time (also denoted by τ_{tr}^e)

`

If the voltage is very small the carriers will recombine before they reach the contact then gain will be

$$\Gamma_G = \frac{\tau}{\frac{L^2}{\mu_e V}} < 1 \quad (15)$$

If the voltage is made Larger, the electrons travel faster than holes, then the gain will be

$$\Gamma_G = \frac{\tau}{\frac{L^2}{\mu_e V}} > 1 \quad (16)$$

but if the voltage is made Larger then gain will be

$$\Gamma_G = \frac{\tau}{\frac{L^2}{\mu_e V}} = 1 \quad (17)$$

And Photocurrent

$$I_{ph} = q\eta \frac{P_{inc}}{h\nu} \frac{\tau}{\frac{L^2}{\mu_e V}} \quad (18)$$

4.1.8 Time response of the photoconductor (AC behavior)

- The time dependent electron concentration is given by

$$\frac{dn}{dt} = \hat{G} - \frac{n}{\tau} \quad (19)$$

τ_{ph} depends on the photoconductor mode of the operation and on the gain

- for low voltage $\tau_{ph} = \tau$ (20)
- for high voltage τ_{ph} =transit time (21)
- for moderate voltage τ_{ph} =Gx$\frac{L^2}{\mu_e V}$ (22)

`

4.1.9 Detectivity

Detectivity (D^*) is a characterization technique known as figure of merit for photodetectors and it is used to characterize performance of these kind of devices. It is defined as the reciprocal of the noise-equivalent power (NEP) however Detectivity is directly proportional to the detector which is more convenient for understanding. The units are given in Jones (J) and 1 J is equivalent to $1cmHz^{1/2}W^{-1}$. Detectivity is described by:

$$D^* = \frac{R(\sqrt{A})}{2q(I_{dark})} \tag{23}$$

Where: R stands for Responsivity, A is the Effective Area, Q isthe electron charge and I_{dark} is thecurrent of the device without light excitation.

4.2 Results

All measurements were performed inside of the chamber of a lakeshore crx-4k probe stage. First the current without light was measured next to it the photocurrent was measured by using two light sources the first one was a Tor Labs DC220 that provides white light also known as broadband, and the other source was a Fianium LLTFCONTRAST which is a tunable laser for this work it was used an electromagnetic wave of 660nm which can be seen as a red laser. All these three measurements where performed by each increment of 50 ˚K from 5.4 ˚K all the way to 350 ˚K. the same processes were applied after adding the Au nanoparticles. After the measurements the equations previously mentioned in 4.1 were performed in order of calculate the performance parameters of the device here developed, before and after plasmonic effect, in order to compare and get a final conclusion. Some results are presented below.

4.2.1 I-V Dark Current Before and After Au Nanoparticles

Dark current is the smallest current that flows through photodetectors even when no photons are interacting with the device. It happens because some charges are generated in the detector (with no light interfering) due to the random generation of electrons and holes within the depletion region. In this case the charge generation rate is related to specific crystallographic defects within the depletion region.

It is also known as reverse bias leakage current and it is presented in all diodes. Because of that Dark current is one of the main sources of noise in image sensors such as charge-coupled-device (CCD) Sensors. Figure 26 shows the dark currents for the device fabricated here, at diferent temperatures, starting from 5.4 Kelvin and increasing temperature each 50 Kelvin degrees all the way to 350˚K this measurement was performed before and after Au Nano-particles (NP). In image "a" which is before Nano-particles, the maximum dark current is 20 V at 300˚K giving a current of $11.98X10^{-7}$ Amperes, meanwhile in "b" (after NP) it is presented a current of $1.20x10^{-4}$ Amperes.

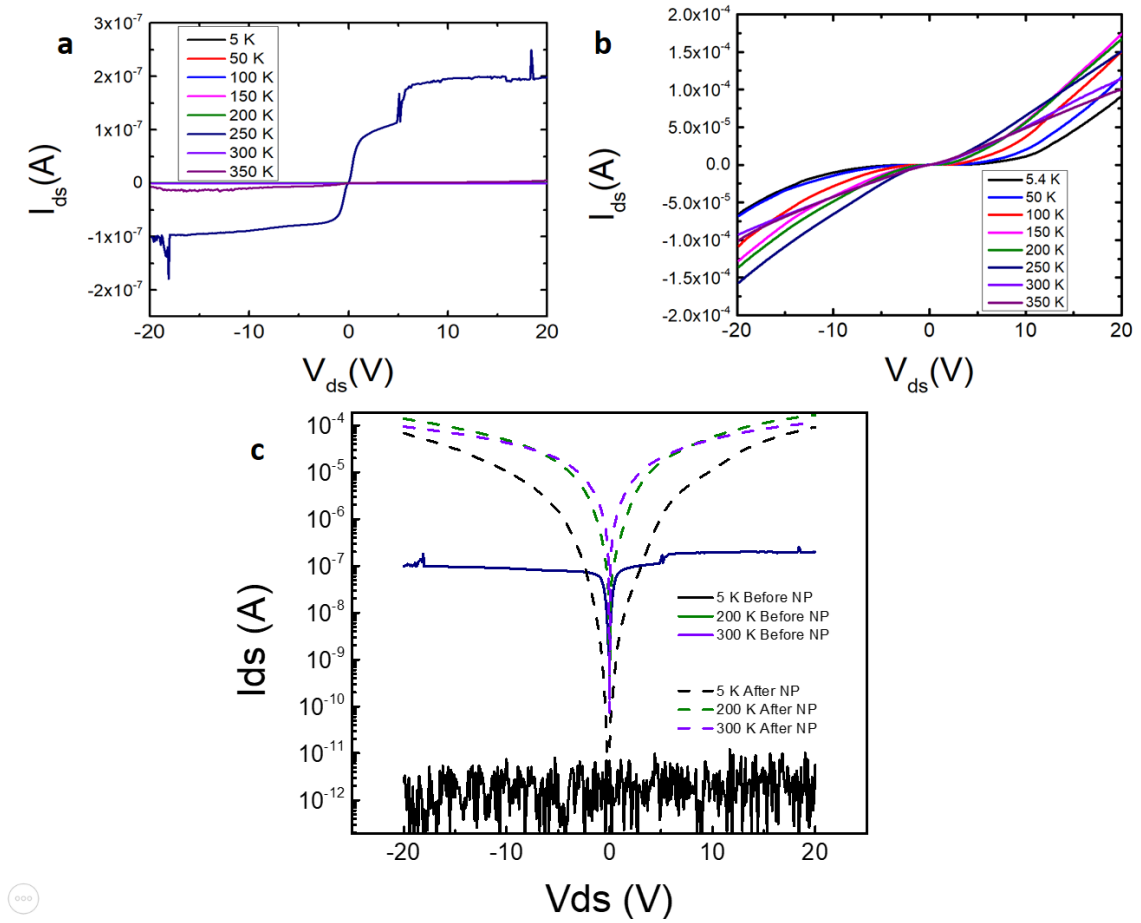

Figure 30. I-V measurement under no illumination (Dark current), a) shows the dark current before Au Nano Particles (NP), b) shows the dark current After Au NP. And c) shows a comparison between Three I-V curves at three different temperatures (5,200 and 300 ˚K) the dash lines are measurements after Gold NP and continuous lines are measurements before Gold nanoparticles.

4.2.2 I-V Broadband Before and After Au Nanoparticles

I-V measurements were performed for the MoS_2 Mechanical exfoliated photodetector device applying two different sources of light, Broadband and 660nm wavelength Laser. in Figure 27 it is presented the I-V curves for broadband, and Laser 660nm from -20V to 20V at 5.4 Kelvin, before nanoparticles (image a) where the highest current obtained was broadband at 20V providing a current of $1x10^{-7}$Amperes meanwhile for measurements after nanoparticles (image b) the highest current obtained was also Broadband at 20V giving a value in current of $2x10^{-4}$ Amperes. The difference is notable due to Plasmonic effect happening thanks to the Gold Nano-particles in the photodetector. In terms of values it was achieved to increase the current of the device about 3 orders of magnitude going t 10nA to 2mA. Since it is hard to appreciate in a decimal scale, image c in figure 27 shows a logarithmic scale where we can see the increment in current of about three orders of magnitude.

Figure 28 presents I-V curves from -20 to 20 volts, before and after NP (images a and b respectively) at 300˚K. in this case the broadband is the source which allows the highest current in 20V, before and after plasmonic effect. In Figure 28 image “a” shows the IV measurements before adding Au NP with maximum current of $2x10^{-7}$Amperes, meanwhile after adding Gold nanoparticles the increment in current goes up to $3.13x10^{-4}$ Amperes due to plasmonic effect. Again, we can observe the same pattern of three orders of magnitude of increment in current by Plasmonic effect. To make it easier to notice image “c” shows a Logarithmic scale of I-V curves before and after Plasmonic effect.

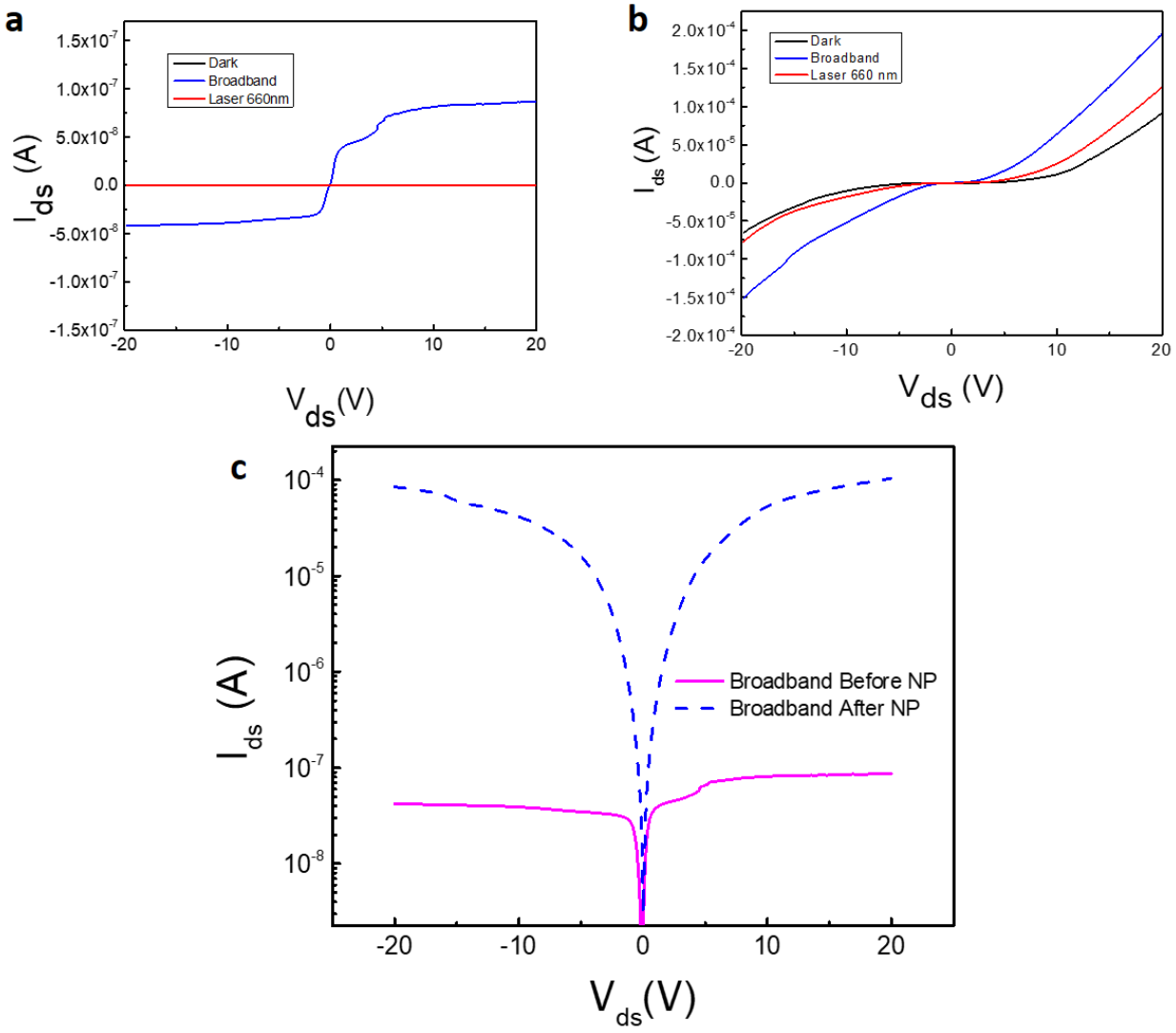

Figure 31. I-V at 5.4 ˚K, a) measurement before Au Nano Particles (NP), b) measurement after Au NP, and c) comparison between broadband before and after NP in logarithmic scale in order to distinguish the difference between both I-V measurements, the pink continuous line represents the measurement before and the blue dashed line represents the measurement after NP.

`

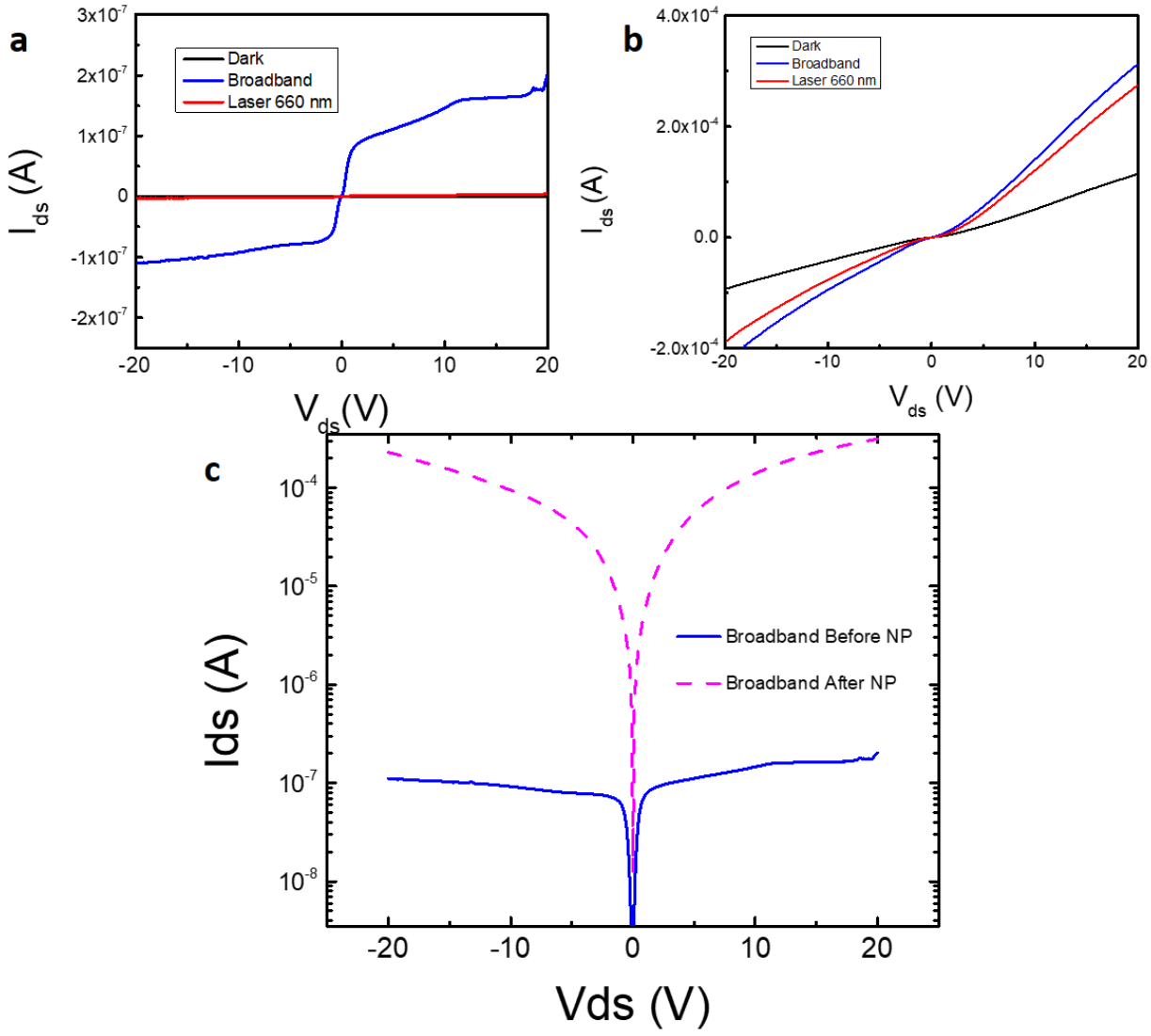

Figure 32. I-V at 300K image a) shows I-V curves of the MoS_2 photodetector before Au Nanoparticles, b) is the IV curve of the same device after coating with Au NP, c) is a comparison between the I-V curves at 300K before and after Au Nanoparticles in Logarithmic scale which allows to notice the improvement in current of 3 orders of magnitude.

`

4.2.3 I-V Laser 660nm Before and After Au Nanoparticles

In spite of the fact that MoS_2 Mechanical exfoliated photodetector shows much better performance with Broadband as light source, it is important to mention that there was also a notable improvement in performance for 660nm Laser source due to plasmonic effect, in this case the current was improved six orders of magnitude. Going from $2.9x10^{-10}$ to $1.25x10^{-4}$ Amperes at 5.4˚K. the same pattern was found for 300˚K, going from $1.2x10^{-10}$ to $1.15x10^{-4}$ Amperes.

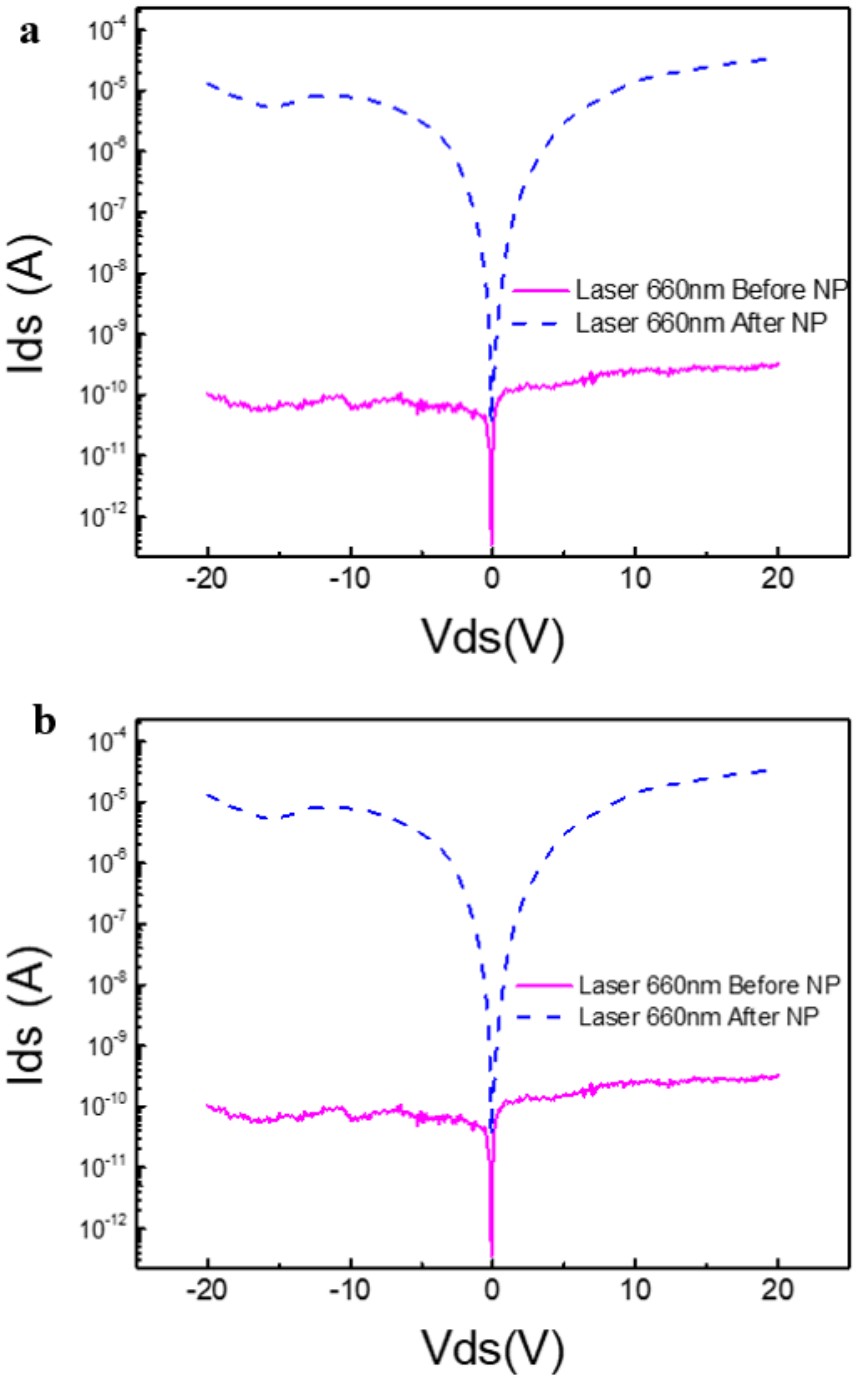

Figure 33. I-V curves of Laser 660nm blue dot line is the measurement after Au NP, and continuous Pink line represents the measurement before Au NP a) at 5.4k and b) at 300K.

`

4.2.4 Photocurrent

Photocurrent (I_{ph}) is defined as the electric current through a photosensitive device. It is given by substracting the Dark current from the total current drain-source (I_{ds}) after applying light to the Photodetector.

$$I_{ph} = I_{ds} - I_{dark} \quad (24)$$

In figure 30 a) there is presented a logarithmic scale plot showing photocurrent versus voltage relationship with and without plasmonic effect at 300 ˚K, with both sources of light (broadband and laser 660nm). The continuous line represents the measurement without Gold NP and the dashed line represents the measurements with plasmonic effect increasing the photocurrent three orders of magnitude and about for Broadband and about 3 orders of magnitude going from $2X10^{-7}$ before Au NP, to $2X10^{-4.}$ Meanwhile for laser 660nm wavelength the increment due to plasmonic effect goes up to 5 orders of magnitude, going from $3.7X10^{-9}$ all the way to $1.6X10^{-4}$.

In particular the mechanism that rules in this MoS2 photodetector is photovoltaic effect due to the metal semiconductor junction, that we can prove by the Schottky diode I-V characteristic curves[54] obtained in this experiment. However, there are other mechanisms contributing to the Photocurrent generation in MoS_2 such as Thermoelectric effect which

Since each IV was measured at different temperatures it was easy to calculate the photocurrent for each temperature under both sources of light (Broadband and laser 660nm wavelength) and then compare them among their analogous after adding Gold nanoparticles. This relationship can be seen in figure 30 image b) where it can be noticed that temperature does affect the behavior of this MoS_2 photodetector because the photocurrent increases as the temperature goes up. The highest values for photocurrent were achieved at 300˚K reaching values of $2X10^{-7}$ for broadband and $3.8X10^{-9}$ for laser 660nm wavelength. An improvement of 3 orders of magnitude is reported here for Broadband ($2X10^{-4}$ A) and five orders of magnitude for laser ($1.6x10^{-4}$) by Plasmonic effect after adding Gold nanoparticles.

`

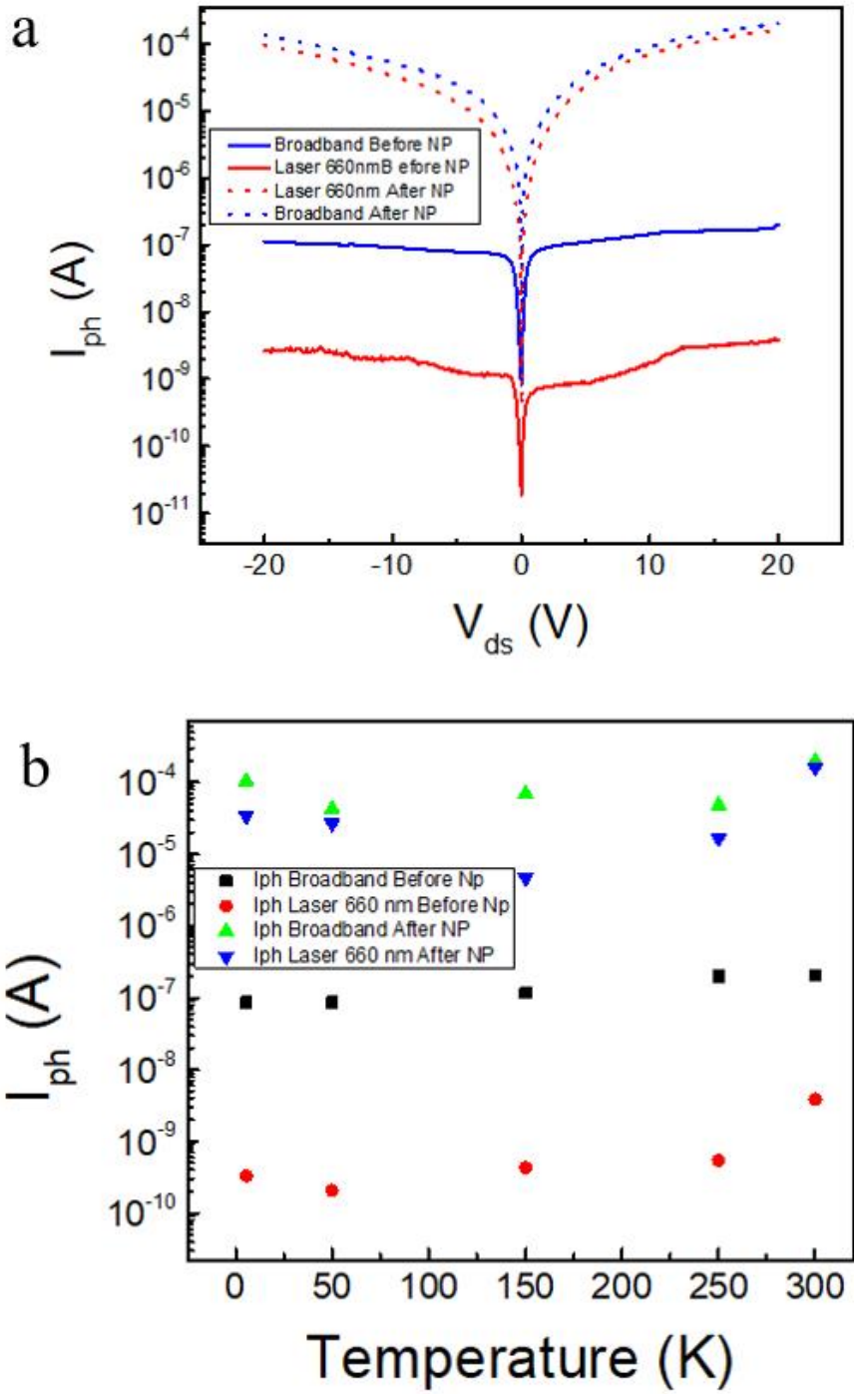

Figure 34. photocurrent plots, a) shows the photocurrent versus Voltage at 300K, b) is the relationship between Photocurrent (I_{ph}) obtained before and after Au NP at different temperature.

`

4.2.5 Photoresponsivity

As mentioned before Responsivity "R" is the ratio of energy in (watts) incident on the photodiode and the photocurrent output (Amperes) it is expressed in A/W and measures the input-output gain of a detector. Responsivity is given by:

$$R = \frac{I_{ph}}{P_{opt}} \tag{25}$$

Also known as external photoresponsivity, expresses the spectral response some MoS2 Fets have reported values of responsivity about mA/W [17], since this is directly proportional to the photocurrent we can imply that the higher the photocurrent the better the performance of a photodetector.

Here it was presented a maximum value in responsivity at 300˚K of $4.9X10^{-5}$ A/W for laser 660nm wavelength and $2.5X10^{-3}$ A/W for broadband before Plasmonic effect. In contrast, after plasmonic effect it was achieved a maximum in responsivity of about 6.5 A/W for broadband and 0.27A/W for the laser, meaning an increment of about five and three orders of magnitude with respect Laser and Broadband sources respectively. These values can be appreciated in Figure 31. Where it is presented the responsivity of the two sources of light, laser expressed in red color and broadband in black color, the same way before and after plasmonic effect are differenciasted because squares are used for calculations before plasmonic effect and circles are used for calculations after plasmonic effect.

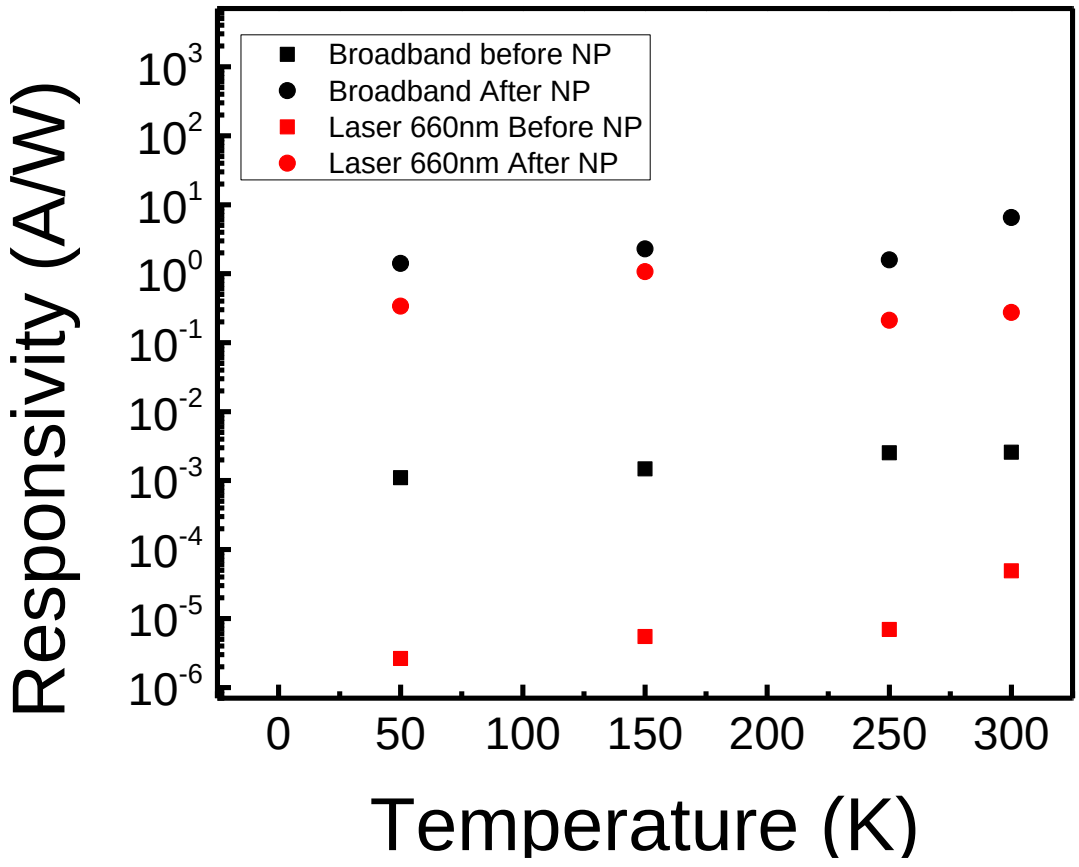

Figure 35. relationship between Responsivity and temperature in color red are expressed the behavior of the laser 660nm of wavelength and color black corresponds to Broadband light source, meanwhile calculations before Plasmonic effect are presented in squares and circles aster Plasmonic effect.

`

4.2.6 Detectivity

It is a figure of merit strongly related to Responsivity, both are directly proportional with each other, and as mentioned before it means that the higher the value of detectivity the better the performance of the photodetector.

Basically, the photocurrent signal increases in proportion to the active optical area (A_{opt}) and in addition the noise current increases with the square root of the product of the active optical area with the bandwidth BW.

As mentioned in 4.1.9 detectivity is given by

$$D^* = \frac{R(\sqrt{A})}{2q(I_{dark})} \tag{26}$$

In units of Jones where 1 Jones = 1 $cmHz^{1/2}W^{-1}$.

In figure 32 it is expressed the relationship between detectivity with respect to the different wavelengths at 300˚K. here it can be seen that the highest values of detectivity are given by the electromagnetic wavelengths 550nm and 800nm. For the first one the value of $3X10^{13}$ Jones was improved to $4.54X10^{15}$ Jones after plasmonic effect. Meanwhile for the 880nm wavelength the value of detectivity was improved from $1.21X10^{13}$ Jones to $8.5X10^{15}$ Jones.

Detectivity in the MoS_2 photodetector here developed without plasmonic effect is represented by color black. Meanwhile color red represents the detectivity after gold nano-particles, presenting plasmonic effect.

`

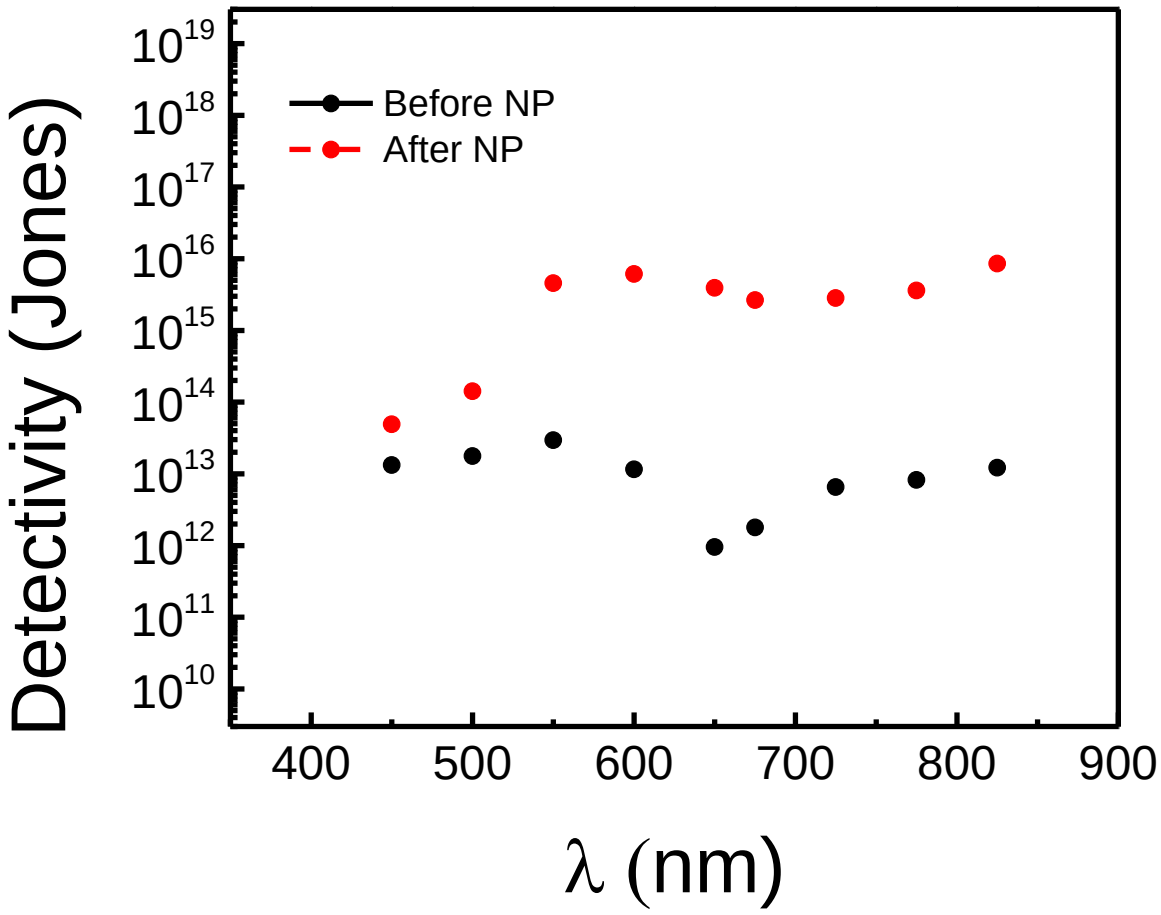

Figure 36. Detectivity relationship with electromagnetic wavelengths, in black are the detectivities before adding gold nanoparticles, meanwhile detectivity influenced by plasmonic effect is represented in red color.

`

4.2.7 External Quantum Efficiency

External quantum efficiency happens to be one of the most important parameters to determine the performance of photodetectors. It is defined as the number of carriers (electron-hole pairs) per second collected to produce the photocurrent divided by the number of incident photons per second. Mathematically it can be seen as:

$$I_{ph} = q\eta \frac{P_{inc}}{hv} \tag{27}$$

A relationship between Quantum Efficiency at different wavelengths is shown in figure 33, where the highest increment is carried out at 550nm wavelength. In this work it was able to achieve an increment in quantum efficiency of 75 times at 550nm wavelength after plasmonic effect. Going from 9.7% efficiency before adding Au Nanoparticles to 735% efficiency after adding Gold nanoparticles due to plasmonic effect.

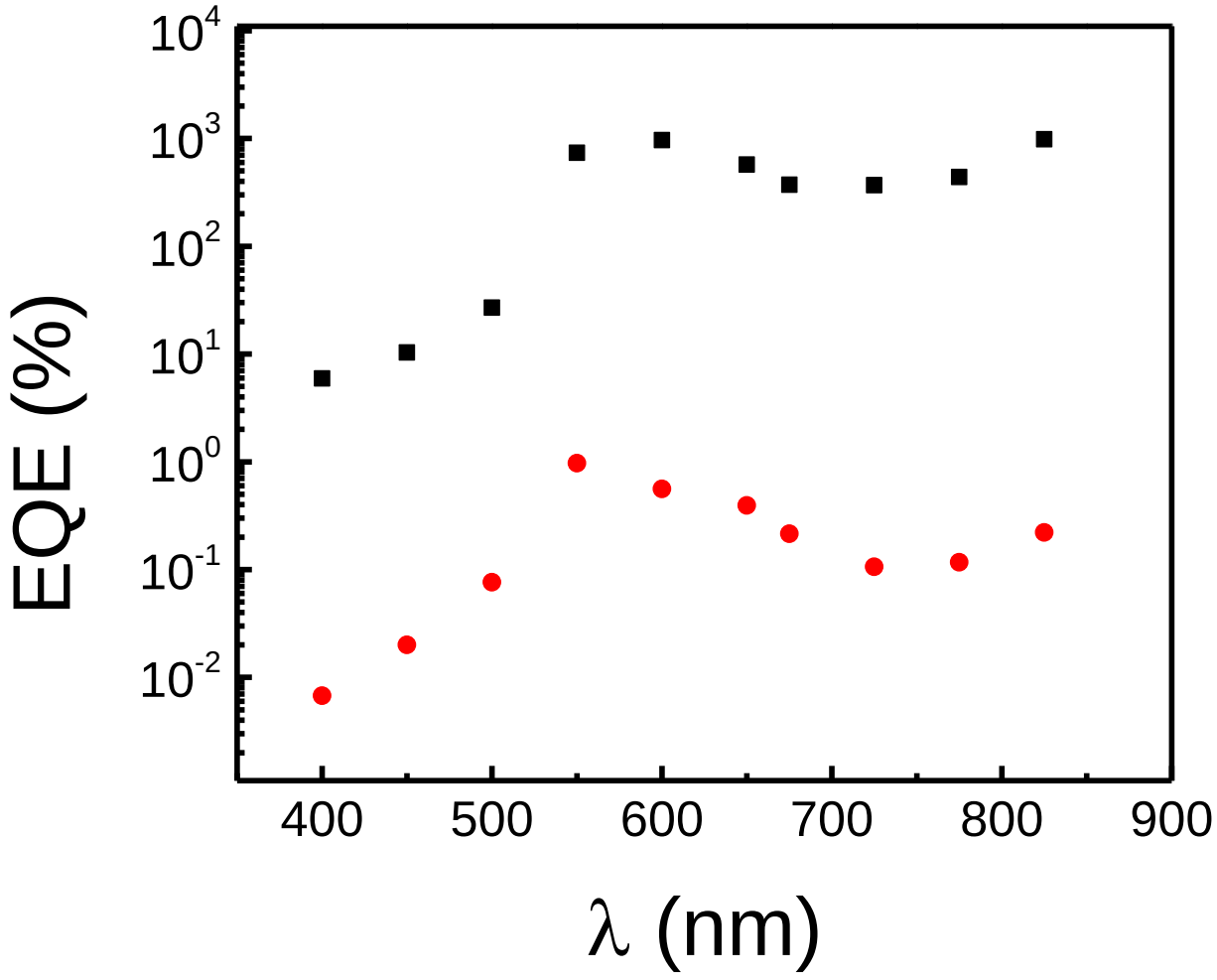

Figure 37. relationship between External Quantum efficiency and wavelength. Black dots represent EQE before plasmonic effect, and red dots represent EQE after plasmonic effect in the MoS2 photodetector.

CHAPTER 5 CONCLUSIONS

In this work a MoS_2 multilayer Photodetector has been fabricated and the performance where improved by taking advantage of the plasmonic effect. For doing so, many scientific articles where reviewed and the most relevant methods where applied, starting from the MoS_2 synthesis methods which covers from mechanical exfoliation to Chemical Vapor Deposition, characterization techniques such as Optical Microscopy, Raman and PL spectrometry, SEM, AFM as well as absorption spectrometry (by UV-Vis cary). Some methods of device fabrication where reviewed and applied such as photolithography, metal contact deposition, transfer of thin films either viscoelastic stamping methods for Mechanical exfoliated films or SiO_2 etching for CVD synthetized thin films. And finally, fundamentals of optoelectronic characterization were explained and performed on the Photodetector here fabricated, such optoelectronic characterization techniques includes the well known as figures of merit of photodetectors such as I-V measurements under light and under no light (Dark current) applied, photocurrent, responsivity, detectivity, and quantum efficiency.

Whit such optoelectrical characterization techniques it was possible to determine the performance of the MoS_2 photodetector here fabricated. Then, by measuring and calculating the optoelectronic phenomena before and after using Au Nanoparticles it was able to determine how the plasmonic effect does affect the performance of the Photodetector. In this case an increase in photocurrent was evidently, which also improved other related characteristics such as Responsivity, Detectivity, and Quantum efficiency for both sources of light either Broadband or Laser 660nm wavelength. In the case of Broadband which happens to have the highest current levels before and after nanoparticles, it was possible to increase the values about three orders of magnitude, going from $2X10^{-7}$ Amperes before plasmonic effect to $2X10^{-4}$ Amperes of photocurrent after plasmonic effect. Conversely for Laser 660nm the improvement in photocurrent was higher, about five orders of magnitude, however these values were below the Broadband ones.

`

Given the outcome of this work, we will be submitting our work for publication in a peer reviewed journal [55].

REFERENCES

[1] W. Shockley and H. J. Queisser, "Detailed balance limit of efficiency of p-n junction solar cells," *J. Appl. Phys.*, vol. 32, no. 3, pp. 510–519, 1961.

[2] L. Rapoport, N. Fleischer, and R. Tenne, "Applications of WS2(MoS2) inorganic nanotubes and fullerene-like nanoparticles for solid lubrication and for structural nanocomposites," *J. Mater. Chem.*, vol. 15, no. 18, p. 1782, 2005.

[3] M. Ablikim *et al.*, "Search for K<inf>S</inf>⁰K<inf>L</inf>⁰ in ψ″ decays," *Phys. Rev. D - Part. Fields, Gravit. Cosmol.*, vol. 70, no. 7, 2004.

[4] A. Magasinski *et al.*, "Toward efficient binders for Li-ion battery Si-based anodes: Polyacrylic acid," *ACS Appl. Mater. Interfaces*, vol. 2, no. 11, pp. 3004–3010, 2010.

[5] S. N. Luo, L. Zheng, A. Strachan, and D. C. Swift, "Reply to 'comment on "Melting dynamics of superheated argon: Nucleation and growth"' [J. Chem. Phys. 126, 034505 (2007)]," *Journal of Chemical Physics*, vol. 126, no. 18. 2007.

[6] a. P. Graham and J. P. Toennies, "Comment on 'Surface diffusion potential energy surfaces from first principles: CO chemisorbed on Pt{110}' [J. Chem. Phys. 111, 9461 (1999)]," *J. Chem. Phys.*, vol. 114, no. 2, p. 1051, 2001.

[7] A. Castellanos-Gomez, J. Quereda, H. P. van der Meulen, N. Agrait, and G. Rubio-Bollinger, "Spatially resolved optical absorption spectroscopy of single- and few-layer MoS2 by hyperspectral imaging," *Nanotechnology*, vol. 27, no. 11, p. 5, 2016.

[8] H. Li *et al.*, "Rapid and reliable thickness identification of two-dimensional nanosheets using optical microscopy," *ACS Nano*, vol. 7, no. 11, pp. 10344–10353, 2013.

[9] Z. He and W. Que, "Molybdenum disulfide nanomaterials: Structures, properties, synthesis and recent progress on hydrogen evolution reaction," *Appl. Mater. Today*, vol. 3, pp. 23–56, 2016.

[10] T. Li and G. Galli, "Electronic properties of MoS 2 nanoparticles," *J. Phys. Chem. C*, vol. 111, no. 44, pp. 16192–16196, 2007.

[11] C. Lee, H. Yan, L. Brus, T. Heinz, J. Hone, and S. Ryu, "Anomalous lattice vibrations of single-and few-layer MoS2," *ACS Nano*, vol. 4, no. 5, pp. 2695–700, 2010.

[12] R. R. Nair *et al.*, "Fine Structure Constant Defines Visual Transparency of Graphene," *Science (80-.).*, vol. 320, no. 5881, pp. 1308–1308, 2008.

[13] J. J. Winnink, "Searching for Structural Shifts in Science : Graphene R & D before and after Novoselov et al . (2004)," in *Proceedings of 17th International Conference on Science and Technology Indicators*, 2012, vol. 2, pp. 835–846.

[14] S. Pillai, K. R. Catchpole, T. Trupke, and M. A. Green, “Surface plasmon enhanced silicon solar cells,” *J. Appl. Phys.*, vol. 101, no. 9, pp. 1–9, 2007.

[15] S. Pillai, F. J. Beck, K. R. Catchpole, Z. Ouyang, and M. A. Green, “The effect of dielectric spacer thickness on surface plasmon enhanced solar cells for front and rear side depositions,” in *Journal of Applied Physics*, 2011, vol. 109, no. 7.

[16] H. A. Atwater and A. Polman, “Plasmonics for improved photovoltaic devices,” *Nat. Mater.*, vol. 9, no. 3, pp. 205–213, 2010.

[17] O. Lopez-Sanchez, D. Lembke, M. Kayci, A. Radenovic, and A. Kis, “Ultrasensitive photodetectors based on monolayer MoS 2,” *Nat. Nanotechnol.*, vol. 8, no. 7, pp. 497–501, 2013.

[18] S. Jeon *et al.*, “Gated three-terminal device architecture to eliminate persistent photoconductivity in oxide semiconductor photosensor arrays,” *Nat. Mater.*, vol. 11, no. 4, pp. 301–305, 2012.

[19] M. Buscema *et al.*, “Photocurrent generation with two-dimensional van der Waals semiconductors,” *Chem. Soc. Rev.*, vol. 44, no. 11, pp. 3691–3718, 2015.

[20] K. S. Novoselov *et al.*, “Electric field effect in atomically thin carbon films.,” *Science*, vol. 306, no. 5696, pp. 666–9, 2004.

[21] R. Ganatra and Q. Zhang, “Few-layer MoS2: A promising layered semiconductor,” *ACS Nano*, vol. 8, no. 5. pp. 4074–4099, 2014.

[22] K. R. Paton *et al.*, “Scalable production of large quantities of defect-free few-layer graphene by shear exfoliation in liquids,” *Nat. Mater.*, vol. 13, no. 6, pp. 624–630, 2014.

[23] S. Najmaei *et al.*, “Vapour phase growth and grain boundary structure of molybdenum disulphide atomic layers,” *Nat. Mater.*, vol. 12, no. 8, pp. 754–759, 2013.

[24] W. Zhang *et al.*, “A one-step approach to the large-scale synthesis of functionalized MoS 2 nanosheets by ionic liquid assisted grinding,” *Nanoscale*, vol. 7, no. 22, pp. 10210–10217, 2015.

[25] D. Xu *et al.*, “Microwave-assisted 1T to 2H phase reversion of MoS2 in solution: A fast route to processable dispersions of 2H-MoS2 nanosheets and nanocomposites,” *Nanotechnology*, vol. 27, no. 38, 2016.

[26] X. Qin, P. Ke, A. Wang, and K. H. Kim, “Microstructure, mechanical and tribological behaviors of MoS2-Ti composite coatings deposited by a hybrid HIPIMS method,” *Surf. Coatings Technol.*, vol. 228, pp. 275–281, 2013.

[27] S. Vishwanath *et al.*, “Comprehensive structural and optical characterization of MBE grown MoSe 2 on graphite, CaF 2 and graphene,” *2D Mater.*, vol. 2, no. 2, p. 24007, 2015.

[28] X. Zhou, B. Xu, Z. Lin, D. Shu, and L. Ma, “Hydrothermal synthesis of flower-like MoS2nanospheres for electrochemical supercapacitors,” *J. Nanosci. Nanotechnol.*, vol. 14, pp. 7250–7254, 2014.

[29] A. Valdivia, D. J. Tweet, and J. F. Conley, “Atomic layer deposition of two dimensional MoS_2 on 150 mm substrates,” *J. Vac. Sci. Technol. A Vacuum, Surfaces, Film.*, vol. 34, no. 2, p. 21515, 2016.

[30] C. Ahn *et al.*, “Low-Temperature Synthesis of Large-Scale Molybdenum Disulfide Thin Films Directly on a Plastic Substrate Using Plasma-Enhanced Chemical Vapor Deposition,” *Adv. Mater.*, vol. 27, no. 35, pp. 5223–5229, 2015.

[31] S. Ijiima, “IIjima, 1991, Helical microtubles of graphitic carbon.pdf,” *Nature*, vol. 354, pp. 56–58, 1991.

[32] P. Karamanis, N. Otero, and C. Pouchan, “Comment on ‘Planar tetra-coordinate carbon resulting in enhanced third-order nonlinear optical response of metal-terminated graphene nanoribbons’ by G.-L. Chai, C.-S. Lin and W.-D. Cheng, J. Mater. Chem., 2012, 22, 11303,” *J. Mater. Chem. C*, vol. 1, no. 17, p. 3035, 2013.

[33] G. Z. Magda, J. Petõ, G. Dobrik, C. Hwang, L. P. Biró, and L. Tapasztó, “Exfoliation of large-area transition metal chalcogenide single layers,” *Sci. Rep.*, vol. 5, 2015.

[34] K. S. Novoselov *et al.*, “Two-dimensional gas of massless Dirac fermions in graphene,” *Nature*, vol. 438, no. 7065, pp. 197–200, 2005.

[35] J. Shi *et al.*, “Controllable growth and transfer of monolayer MoS2 on Au foils and its potential application in hydrogen evolution reaction,” *ACS Nano*, vol. 8, no. 10, pp. 10196–10204, 2014.

[36] J. F. Shackelford and R. H. Doremus, *Ceramic and glass materials: Structure, properties and processing*. 2008.

[37] A. O’Neill, U. Khan, and J. N. Coleman, “Preparation of high concentration dispersions of exfoliated MoS 2 with increased flake size,” *Chem. Mater.*, vol. 24, no. 12, pp. 2414–2421, 2012.

[38] B. D. Keller, A. Bertuch, J. Provine, G. Sundaram, N. Ferralis, and J. C. Grossman, “Process Control of Atomic Layer Deposition Molybdenum Oxide Nucleation and Sulfidation to Large-Area MoS2 Monolayers,” *Chem. Mater.*, vol. 29, no. 5, pp. 2024–2032, 2017.

[39] X. Ling *et al.*, “Role of the Seeding Promoter in MoS 2 Growth by Chemical Vapor Deposition,” *Nano Lett.*, vol. 14, no. 2, pp. 464–472, 2014.

[40] G. Alberto and L. Saenz, “SYNTHESIS , DEVICE FABRICATION AND CHARACTERIZATION OF TWO-DIMENSIONAL MOLYBDENUM DISULFIDE.”

[41] E. Incident *et al.*, “Optical Detectors Photodiodes and Phototransistors – Photodiodes are designed to detect photons and,” *Appl. Phys. Lett.*, vol. 102, no. 1, pp. 1–5, 2013.

[42] J. F., *Fundamentals of linear electronics: integrated and discrete.* .

[43] K. M. McCreary *et al.*, “The effect of preparation conditions on raman and photoluminescence of monolayer WS2,” *Sci. Rep.*, vol. 6, no. October, pp. 1–10, 2016.

[44] D. Ma *et al.*, “Etching-free transfer of wafer-scale MoS2 films,” *ArXiv e-prints*, 2015.

[45] Z. Yin *et al.*, “Single-layer MoS2 phototransistors,” *ACS Nano*, vol. 6, no. 1, pp. 74–80, 2012.

[46] D. R. Lide, “CRC Handbook of Chemistry and Physics, 84th Edition, 2003-2004,” *Handb. Chem. Phys.*, vol. 53, p. 2616, 2003.

[47] P. Rai-Choudhury, M. A. McCord, and M. J. Rooks, “Handbook of microlithography, micromachining, and microfabrication. Chapter 2 E. beam lithography,” *Handb. Microlithogr. Micromach. Microfabr.*, vol. 1, p. 692, 1997.

[48] A. Castellanos-Gomez *et al.*, “Deterministic transfer of two-dimensional materials by all-dry viscoelastic stamping,” *2D Mater.*, vol. 1, no. 1, pp. 1–34, 2014.

[49] S. A. Maier, *Plasmonics: Fundamentals and applications*. 2007.

[50] A. Ahmadivand, N. Pala, and D. Ö. Güney, “Enhancement of photothermal heat generation by metallodielectric nanoplasmonic clusters,” *Opt. Express*, vol. 23, no. 11, p. A682, 2015.

[51] S. H. Lim, D. Derkacs, and E. T. Yu, “Light scattering into silicon-on-insulator waveguide modes by random and periodic gold nanodot arrays,” *J. Appl. Phys.*, vol. 105, no. 7, 2009.

[52] W. Du, H. Inokawa, H. Satoh, and A. Ono, “Single-photon detection by a simple silicon-on-insulator metal-oxide-semiconductor field-effect transistor,” *Jpn. J. Appl. Phys.*, vol. 51, no. 6 PART 2, pp. 3–7, 2012.

[53] M. J. Deen and P. K. Basu, *Silicon Photonics: Fundamentals and Devices*. 2012.

[54] Z. M. Wang, *MoS2: Materials , Physics , and Devices*. 2014.

[55] A. B. K. C. de Anda, G. Saenz, “Enhancement of optical absorption properties of 2D MoS2 for photodetectors with plasmonic effects in Au nanoparticles”,” *Nanoscale*.

VITA

Carlos was born and raised in Puebla City, Mexico. he got his B.S. in Mechatronics Engineering in 2012 from the "Universidad del Valle de Mexico" (UVM). Due to his passion for Technology he has been actively participating in conferences and workshops in robotics and MEMS (Micro Electro Mechanical Systems). In Fall 2015 he joined the Department of Electrical Engineering at UTEP to continue his way to Nanotechnology specialization.

He conducted research toward his Master's degree as a Research Assistant when he joined Prof. Kaul's research group at UTEP in Fall 2016. His research has focused on MoS2 synthesis for opto-electronic devices. The outcomes from his MS research have been showcased at international conferences such as the Materials Research Society meeting, HENAAC, and there will be a peer reviewed journal article being submitted for publication shortly.

This thesis/dissertation was typed by Carlos Francisco de Anda Orea.

Contact information: cfdeandaorea@miners.utep.edu or cfd.andor@gmail.com

`